UNIVERSITY OF CALIFORNIA
RIVERSIDE

Drop Impact Behaviors for Cooling Applications

A Thesis submitted in partial satisfaction
of the requirements for the degree of

Master of Science

in

Mechanical Engineering

by

Cynthia Ogechi Ajawara

June 2015

Thesis Committee:

Dr. Guillermo Aguilar, Chairperson
Dr. Marko Princevac
Dr. Lorenzo Mangolini

The Thesis of Cynthia Ogechi Ajawara is approved:

_____

_____

_____

Committee Chairperson

University of California, Riverside

Acknowledgment

I would like to thank Darren Banks for his advice and guidance throughout the project lifetime, and Antonio Cervantes, Hamza Surti, Molly Daniels, Rafael Sanchez, and Jonathan Campoa for their assistance in the laboratory. I would also like to thank Anthony Fong for his constant machining assistance.

I would like to thank Dr. Guillermo Aguilar for his support and guidance.

Thank you to the University of California Riverside Graduate Division and Xerox Corporation for the student support.

Finally, I would like to extend a big thank you to my family and friends for all their support throughout this journey.

ABSTRACT OF THE THESIS

Drop Impact Behaviors for Cooling Applications

by

Cynthia Ogechi Ajawara

Master of Science, Graduate Program in Mechanical Engineering
University of California, Riverside, June 2015
Dr. Guillermo Aguilar, Chairperson

The cooling behavior of an impacting single droplet and train of droplets on a heated substrate (T = 60ºC) for various pool conditions is explored. The effects of several variables such as impact velocity, droplet diameter, pool depth, and impact frequency on the cooling dynamics are explored. Fast response resistance temperature detectors (RTD) embedded at the surface of the aluminum substrate allows for temperature measurement below the droplet impact. A high speed video camera recorded the dynamics of cavity formation within the pool upon the impact of falling droplets. Droplet diameter and

impact velocity were also measured using the high speed video. The instantaneous heat flux and net heat extraction at the surface were obtained using a finite-time step integration of Duhamel's theorem.

Heat transfer appears to be maximized within an intermediate pool depth for the single droplet impacts. At this intermediate pool depth, the impact crater almost reached the pool bottom, suggesting that cold droplet fluid made contact with the substrate, maximizing the cooling effect. Outside this intermediate pool depth, the heat flux appears to decrease. At the lower pool depth, cold droplet fluid is pushed away from the measurement point once the cavity reaches the substrate. Above the optimal pool depth, the droplet does not enter the crater formed by the previous droplet, preventing it from reaching the substrate. For a train of droplets, there seems to be several regions where the heat flux is further reduced due to collision of droplet with emerging jet. It was also found that dry surface provides better heat flux with the heat flux decreasing with formation of thin film. In regards to multiple RTDs, the farther the RTD is from the point of impact, the lower the cooling effects.

Table of Contents

List of Figures

Nomenclature

U	Velocity
d	Diameter
ρ	Density
v	Kinematic viscosity
μ	Dynamic viscosity
f	Frequency
σ	Surface tension
L	Characteristic length
T	Temperature
t	Time
τ	Reference time
z	Vertical coordinate
k	Thermal conductivity
c	Specific heat
q''	Heat flux per unit area
q	Overall heat extraction
r	Radius
$t_{capillary}$	Capillary time
θ	Dimensionless temperature
δ	Dimensionless distance
T_d	Droplet temperature

T_s	Substrate temperature
Re ($\boldsymbol{Re} = \frac{\boldsymbol{Ud}}{\boldsymbol{v}}$)	Reynolds number
We ($\boldsymbol{We} = \frac{\boldsymbol{\rho U^2 d}}{\boldsymbol{\sigma}}$)	Weber number
St ($\boldsymbol{St} = \frac{\boldsymbol{fd}}{\boldsymbol{U}}$)	Strouhal number

Chapter 1 Motivation and Introduction

1.1 Motivation

There are several liquid cooling methods available today for thermal management in electronic systems. These liquid cooling methods include spray cooling, single-phase liquid cooling in micro channels, thermosyphons, immersion flow boiling, jet impingement cooling, and heat pipes [1-6]. Among these, spray cooling is one of the most potent cooling techniques available. It applies a combination of convection and phase change using a small liquid volume to achieve extraordinarily high heat fluxes. Spray cooling can produce heat fluxes greater than 100 W/cm^2 under ideal conditions [7]. Mudawar showed that sprays uniformly cool a wider area than jet impingement and exceed the optimum heat flux of submersion boiling within the same temperature range [8].

Sprays provide a unique combination of desirable cooling characteristics: high heat transfer rate with relatively little fluid surface, uniform surface cooling, low droplet impact velocity and impact pressure, and the elimination of unwanted temperature overshoot [7]. Spray thermal management is used in electronics, food processing, and dermatology, among many others. Spray cooling is currently used to cool the super computer model CRAY X-1 as well as high power laser diodes [9]. Aguilar, et al. used cryogen sprays to cool skin that is undergoing port wine stain laser treatment [10-12]. Kim, et al. studied the use of spray mist in fire suppression [13].

The cooling effectiveness of different fluids, ranging from water to diesel fuel, was explored by Arcoumanis, et al [14]. The influence of impact conditions such as

surface roughness [15], surface tension, viscosity [16], and environmental conditions such as ambient pressure [17] have also been explored.

Sprays contain thousands of droplets, each affected by atomization and impact conditions – for example, the droplet frequency can change as the spray develops, the film thickness on the surface can build up, or droplet size distribution can change. The goal of this study is to establish a framework for optimizing the cooling effectiveness of sprays using the impact fluid and thermal dynamics of single droplet and trains of droplets over a range of impact frequencies. The study of droplet impact behavior will help to understand the underlying mechanics in spray cooling. Connecting a single droplet impact behavior to the cumulative spray effects is the focus of this study.

1.2 Droplet Impact Dynamics and Heat Transfer

The starting point in the analytical study of spray dynamics has been the behavior of a single droplet impacting a surface. Over the last century, many studies have been performed on droplet impact behavior, pioneered by Worthington with milk droplets falling into pools of water [18]. He used milk drops for imaging contrast and found that there is a hollow crater that is formed within the liquid surface upon impact. He observed that, the water and milk do not immediately mix, producing an elevated crown of water from the surface with the milk forming fingers at the tip of the crown [18]. Worthington also compared observations of liquid droplet impacts into pools with solid sphere impacts [19]. In Allen's 1974 letter, he discussed the conditions – i.e. fluid densities, wavelength of the interfacial waves, impact velocity, and drop acceleration due to gravity that could lead to splashing and how these conditions all play a role in overcoming the surface

tension [20]. Rein in his 1993 review article chronicled the observed outcomes of a droplet impacting on a pool- notably bouncing, coalescing, spreading, and splashing- and related these behaviors to the Weber number, a ratio of inertia to surface tension (Equation 1) [21]. Some of the phenomena mentioned above can be seen in Figures 1a, b, and c. Wang et al. looked at the critical Weber number to achieve splashing when a droplet impacts a surface, finding that the criteria is unchanged when the surface is a solid or a very thin liquid film [22].

$$We = \frac{\rho U^2 d}{\sigma} \tag{1}$$

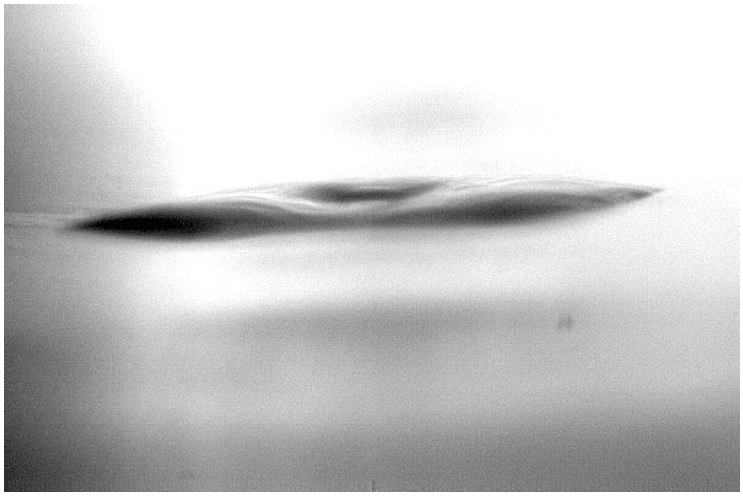

a. Coalescence

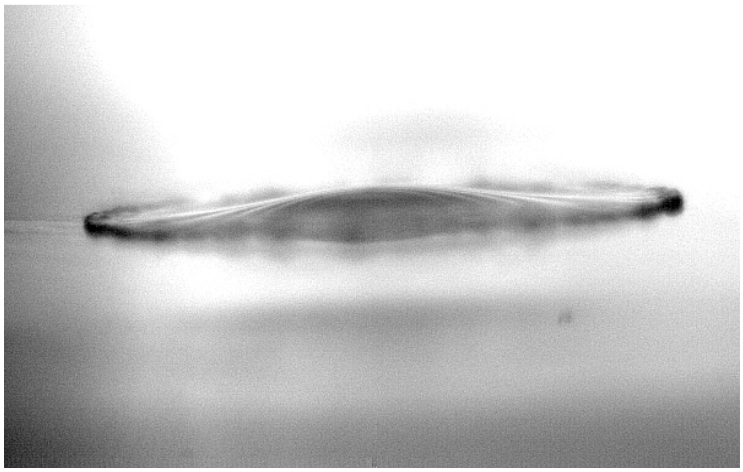

b. Spreading

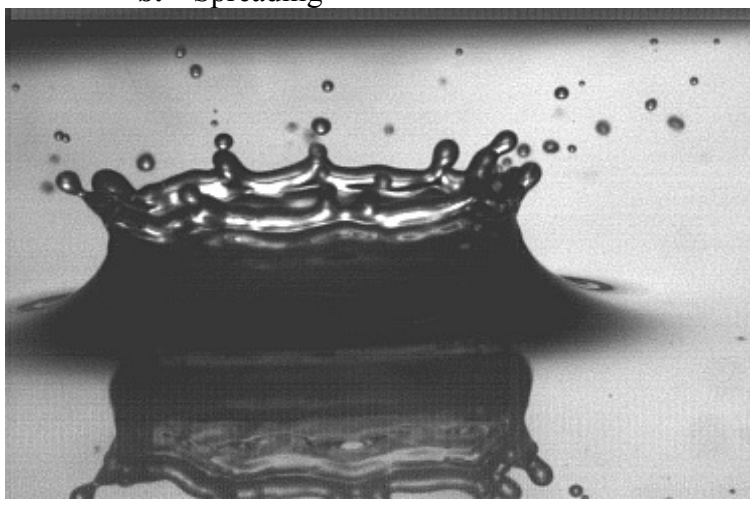

c. Splashing

Figure 1: Images of coalescence, spreading, and splashing taken using high speed video

Yarin and Weiss examined the behavior of droplets falling onto a dry surface, categorizing splashing by the Capillary number (Equation 2) instead of the more commonly used Weber and Reynolds numbers, as both viscosity and surface tension each play roles in splashing dynamics [23]. They determined that splashing was dependent on the spreading liquid lamella layer rather than the initial dynamics of the droplet's impact [23]. Tropea and Marengo explored the impact of drops on films where they formulated a correlation (Equation 3) to determine the threshold for splashing [24]. Their correlation takes into account Weber and Ohnesorge numbers, relation of viscous forces to surface tension and inertial forces (Equation 4), and equates it to a value K that is obtained by multiplying the Ohnesorge and Reynolds numbers (Equation 5) [24]. Reynolds number is the ratio of inertial forces to viscous forces (Equation 6).

$$Ca = \frac{\mu U}{\sigma} \tag{2}$$

$$WeOh^{-0.4} = K \tag{3}$$

Where K < 657 results in complete deposition and K > 657 results in splashing [24].

$$Oh = \frac{\mu}{\sqrt{\rho\sigma L}} = \frac{\sqrt{We}}{Re} \tag{4}$$

$$K = OhRe^{1.25} \tag{5}$$

$$Re = \frac{Ud}{v} \tag{6}$$

Yarin later provided an extensive review of modern droplet impact studies [25]. In his review, he discussed recent findings concerning droplet impact onto thin films and dry surfaces and the transitions between the observed phenomena categorized by Rein in his 1993 paper, as well as several dynamics that had been discovered since [25]. Huang, et al. explored the phenomena that occur using different fluids, pool thicknesses, droplet velocities, and sizes [26]. They discovered that for a thin film liquid surface, jetting is restricted because there is little room for vertical motion during the impact cavity collapse [26]. A new correlation (Equation 7) was developed for the transition between coalescence and splashing in a deep pool. It used the Weber and Reynolds numbers rather than the previous Weber and Ohnesorge numbers combination developed by Tropea and Marengo (Equation 3) [26].

$$We^{0.375}Re^{0.25} = 70 \tag{7}$$

Previous studies conducted by the Banks, et al. reported several phenomena that will be briefly discussed [16]. The impact behaviors observed in the droplet study are: 1) coalescence, 2) prompt splash, 3) crown formation, and 4) crown splashing. Coalescence, crown formation, and crown splashing were phenomena previously reported in Yarin's 1993 review. Coalescence is defined as the absence of crown formation where the droplet impacts the surface and immediately recedes to a resting position without rising above the film. Prompt splashing, shown in Figure 2, occurs when upon impact; secondary droplets are released from the impact point. Crown formation, Figure 3, is defined by the vertical elevation of fluid above the surface of the film. When secondary droplets are

ejected from this elevated fluid, they are referred to as crown splash. These phenomena especially crown formation and crown splashing were proven relevant to the study of droplet trains and their cooling behaviors.

In the study, the group investigated the effects of viscosity of both the film and drop on drop impacts on liquid films. The fluids investigated included FC-72, water, 60% aqueous glycerol, 85% aqueous glycerol, and pure glycerol [16]. The thresholds of splashing were investigated and related to Weber and Ohnesorge numbers [16]. For water droplets, they reported a low crown splashing Weber threshold of 200 with crown formation at 100 [16]. For water, the higher the viscosity of the film, the less chance of crown formation and splashing. In other words, a higher Weber number is needed for splashing to occur [16].

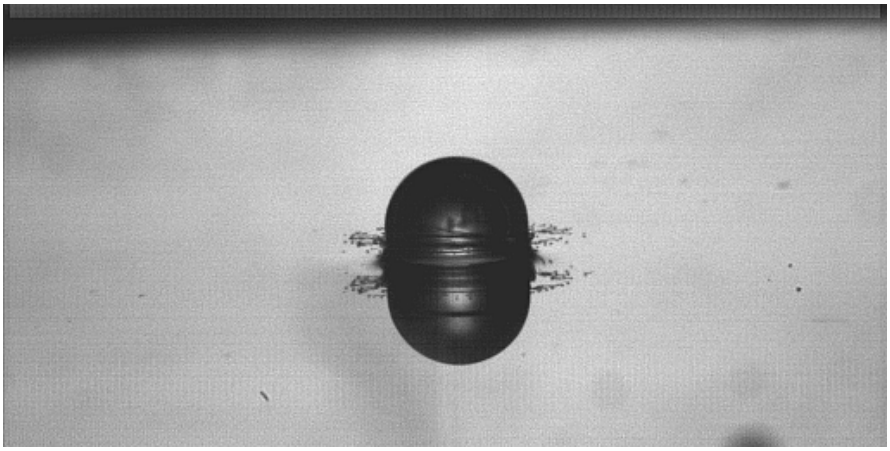

Figure 2: Prompt Splashing

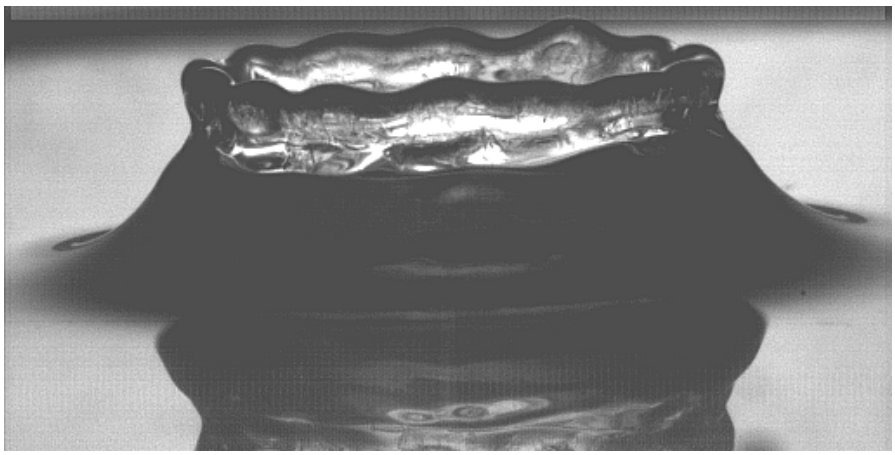

Figure 3: Crown

Banks, et al. have studied the oscillations that occur when a drop impacts on dry surfaces, finding that hydrophobic surfaces promote this oscillation while hydrophilic ones arrest droplet motion quickly [27]. Effects of droplet impact velocity, kinematic viscosity, and surface tension were investigated in correlation to oscillations. They found that oscillations will last longer if the fluid is less viscous, and that a slower oscillation and damped motion occur at higher velocities and on hydrophilic surfaces [27].

Computational and theoretical models have been developed to simulate droplet impact. Weiss et al. investigated the role of gravity and surface tension in crown formation, jetting, bubble entrainment, and necking and reported that lower surface tension creates conditions where the cavity-collapse jet is thinner and faster and higher surface tension damps jetting behavior [28]. Bussmann et al. also provided a numerical simulation of droplet impacts, looking at heptane, water, and molten tin and the different phenomena such as fingering and splashing that arise upon impact [29]. They reported

that fingering and eventually splashing occur as velocity is increased [29]. Trujillo et al. modeled the crown formation behavior caused by a droplet splashing upon impact and reported good agreement by previously obtained splashing thresholds by Yarin and Weiss in their 1995 paper [30]. They also reported that the radius of the crown is dependent on the velocity across the crown and the jump of film height [30].

Fedorchenko and Wang experimentally and theoretically studied the region of splashing where they discovered that the maximum cavity radius and cavity collapse time is dependent on the dimensionless capillary length and Froude number [31]. At Weber number less than two, dimensionless capillary length greater than one, and Froude number between 0.1 and 200, bouncing, floating, and coalescing were present leading to secondary droplet formations [31]. Liu, et al. carried out experimental and numerical simulation studies on droplet impacts on solid surfaces focusing on the splashing phenomena [32]. In the numerical solution study, they reported a decrease in Capillary threshold for splashing in sub-atmospheric pressure [32]. Liang, et al. numerically simulated droplets impacting on a film focusing on the crown behavior and bubble entrapment [33]. The study showed that a decrease in dimensionless film thickness results in an increase of crown diameter and has no correlation to the Weber number [33].

Studies have also been done on the cooling effects of single droplets. Senda et al. studied the heat transfer effectiveness of a droplet impinging on a hot surface [34]. They characterized the thresholds for nucleate boiling, transition boiling, and film boiling while determining how effective each phase is to cooling [34]. Di Marzo, et al. provided

an experimental and theoretical model of droplets that are gently deposited on semi-infinite solid [35]. In that study, they provided models for determining the constant heat flux and thermal transient behavior of droplets for evaporative cooling [35]. Aguilar, et al. experimentally and theoretically studied droplet properties in a cryogen spray where they investigated the droplet diameter, evaporation rate, and temperature for spray optimization [36]. Vu, et al. explored single droplet cooling in shallow heated pools and reported secondary cooling effects, delayed slightly after impact of the droplet into the pool, due to droplet fluid deposition [17].

In their study of a train of droplets impacting on a dry surface, Yarin and Weiss found that there is a formation of unsteady crown from which a jet is formed from the cusps due to a free rim at the top of the crown [23]. A recent study by Lewis, et al simulated cooling behavior of impinging droplet trains and free surface jets over heated and pre-wetted surface and concluded that higher heat transfer coefficient was achieved by the jet due to its smoother hydrodynamic and thermal transition conditions [37]. Trujillo, et al. reported a similar finding to Yarin and Weiss in their 1995 paper where they observed a quasi-steady cavity within a pool that develops [38]. This quasi-steady state occurs when the droplet frequency is high enough that each successive droplet impacts within the cavity of the previous. The walls of the cavity are thus pushed outward radially before cavity can collapse, leading to a cavity diameter that fluctuates around a constant mean [38]. For Trujillo's study, kHz impact frequencies were used with droplet diameters in the order of microns. Heat fluxes ranging from 5 to 35 W/cm^2 were observed, increasing with droplet frequency [38]. This study experimentally builds upon

Lewis, et al.'s work, extending to larger (>1 mm diameter) droplets and lower (0.5-30 Hz) frequencies. The intent is to provide detailed insight into the interactions between successive droplets that contribute to the heat transfer produced on impact.

The thermal and hydraulic phenomena produced by droplet trains upon impact have been studied by Soriano, et al [39]. In that study, the effects of impact frequency, droplet spacing, and droplet size on fluid dynamics and cooling were examined. The highest rate of heat transfer was found to occur with a high radial velocity thin film. The results also showed that for the most effective cooling, the impact crater should not be disturbed by the impact of neighboring droplets; in essence, there is a minimum radial spacing between droplets to achieve the highest heat flux [39]. The conditions that produce craters during droplet impingement into pools have been investigated by Fest-Santini, et al [40]. In the study, the pool temperature was varied and the droplet temperature kept constant to study the conditions needed for a crater to form. They found that periodic ejection of secondary droplets within the crater affects the shape of the crater, and that this ejection motion is more likely to occur at higher temperatures [40].

Most studies measure heat flux only at the point of impact; examining the cooling effects that occur radially outward is relatively rare in literature. Anderson and Ortega experimentally investigated the single phase and evaporative regimes of droplets impinging on a heated surface [41, 42]. Droplets were transported by a gas stream and multiple thermocouples placed in a straight line with known separation to study the spreading and cooling rates of droplets impacting a heated surface [41, 42]. They

reported that an increase in the maximum spreading diameter and instantaneous heat transfer coefficient were contributed to the presence of the air jet [41]. They also discovered during the study that maximum heat transfer was achieved when the droplet reaches its equilibrium film diameter (where the film has stopped receding) [41].

The purpose of this study is to comprehensively investigate the heat transfer and droplet train dynamics to better understand spray cooling. This will be done by studying single droplets and droplet trains impacting on a dry solid surface and liquid pools with a range of depths. The first objective is to characterize the initial cavity growth and collapse from a single droplet as well as droplet trains. The second objective will be to investigate the cooling behavior of single droplets and train of droplets of water impacting on dry surface and varying pool depths of water using single and multiple resistance temperature detectors (RTDs) for temperature readings. The impacts of droplet trains over a range of frequencies are observed as they initiate and develop towards the quasi-steady-state conditions observed by Trujillo, et al, in the context of the observed single droplet cavity dynamics [38].

To characterize and compare the heat transfer of droplet trains, a comprehensive experimental system is being developed. A droplet generator produces trains of millimeter-scale droplets that impact a heated substrate. High speed video observes the fluid dynamics surrounding the impact. Multiple temperature sensors embedded within the substrate provide point and radial measurements of temperatures. The temperature

record and the video are synchronized such that observed fluid and cavity dynamics can be related to specific points in the temperature record.

Chapter 2 Experimental Setup

Figure 4 shows the droplet production and measurement setup. Droplets and droplet trains are produced using a pneumatic solenoid microliter valve (740V, Nordson EFD, USA). The valve is opened by a pneumatic controller (Valvemate 7000, Nordson EFD, USA) triggered by a programmable microcontroller (Arduino Uno R3). The microcontroller can produce voltage pulses with a time resolution on the order of microseconds at set frequencies, and those pulses trigger the valve to open for a prescribed time. The valve is fed from a pressurized liquid reservoir. When actuated, the valve releases pressurized liquid through a steel needle (outer diameter 3.15 mm, inner diameter 2.50 mm, length 110 mm) and a droplet forms at the tip of that needle. After a set time, the valve closes and liquid ceases passing through the needle. When the droplet is large enough, gravity overcomes the surface tension holding the droplet to the needle and the droplet falls. The valve's duty cycle is calibrated to produce one droplet per trigger. Thus, the valve’s cycling frequency corresponds to the droplet frequency. The setup is capable of producing droplet trains with frequencies of up to approximately 50 Hz.

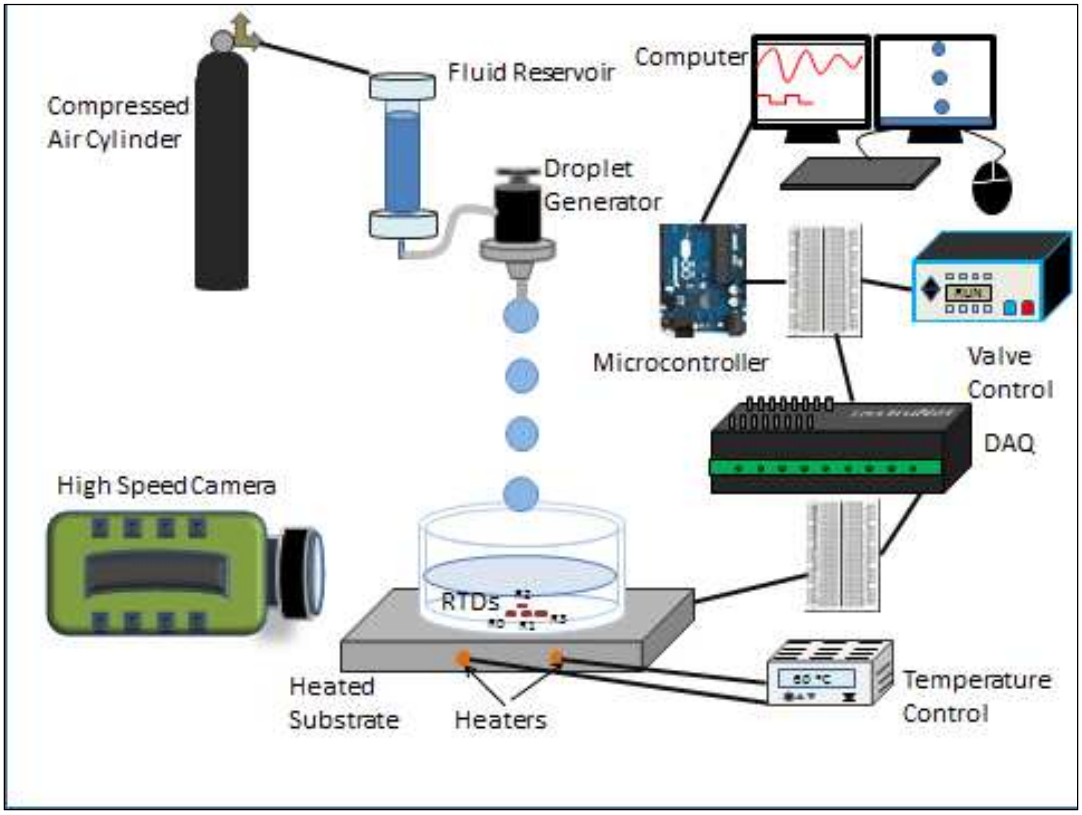

Figure 4: Experimental Setup

The pool and droplets consist of deionized water (study-relevant properties listed in Table 1. Droplets freefall from the needle when they reach a diameter of 4.6±0.1 mm and the impact velocity is 2±0.05 m/s. This results in an impact Weber number of 270 and an impact Reynolds number of 10337. The Strouhal number is defined by Equation 8

$$St = \frac{fd}{U} \qquad (8)$$

Where U is the velocity, d the diameter, and f is drop-generation/impact frequency. For droplet trains up to 32 Hz, it ranges from $0.00115 < St < 0.0736$.

Density: ρ	998 kg/m^3
Kinematic Viscosity: ν	$8.9 \cdot 10^{-7}$ m^2/s
Surface Tension: σ	0.072 N/m
Thermal Conductivity: k	0.5985 W/m·°C
Specific Heat: c	4184 J/kg·°C

Table 1: Properties of deionized water.

The impact substrate consists of an aluminum plate, heated by resistance heaters from within. The heaters are regulated by a temperature controller (Omega CSC32) which receives feedback from a thermocouple placed within the pool away from the impact location. A channel in the face of the aluminum has been filled with cast epoxy resin to hold multiple fast-response resistance temperature detectors (RTD) at the level of the substrate surface. Glass walls surround the plate, retaining a pool of liquid on the aluminum substrate while allowing video recording of the plane of impact. The glass walls are 46 mm tall and have an inner diameter of 116 mm and an outer diameter of 124 mm. The impact is centered within the pool and the length scales of the observed phenomena are typically <20 mm, so the wall effects can be reasonably neglected. For this study, the focus is on the heat transfer induced at the substrate, so the focus is on shallow pools, with depth ranging from dry surface to 15 mm (approximately 3 times the droplet diameter).

2.1 Droplet Pool Design

2.1.1 First generation

First generation was made up of a substrate, pool walls, and two heaters. The substrate consisted of a circular aluminum disk of diameter 100.97 mm and a thickness of 8.82 mm. The face of the aluminum plate was covered with cast epoxy resin. An acrylic

cylinder was used for the walls in order to contain the pool of liquid used for the experiments. The circular aluminum disk is then attached to an aluminum plate with length of 178 mm, width of 127 mm and a height of 15 mm. this rectangular plate is then attached another rectangular plate with the same dimensions.

2.1.2 Second Generation

An RTD was introduced for the second generation of the design. The RTD allowed for the measurement of temperature at the point of contact. A square substrate of dimensions 114 x 114 mm made of aluminum is mounted on top of a rectangular aluminum plate with a length of 178 mm, a width of 127 mm and a thickness of 15 mm. A channel in the face of the substrate, filled with cast epoxy resin, holds a fast-response resistance temperature detector (RTD) flush with the substrate surface. Glass walls surround the plate, retaining a pool of liquid on the substrate and allowing video recording of the plane of impact. The glass walls are 50 mm tall. Resistance heaters in the lower plate heat the substrate from below.

2.1.3 Third Generation

The third generation of the droplet pool featured multiple RTDs embedded into a T-shaped channel (Figure 5). The purpose of the new design was to capture temperature measurements surrounding the point of contact. This new design measures the cooling behavior of the droplets radially outward from the impact as they spread and recede. The substrate is a square base, 126 x 126 mm of aluminum. The square base was machined to have an elevated circle with a diameter of 112 mm and 1.17 mm thickness, raising the impact surface for better video visibility. The pool wall is cylindrical glass 46 mm high,

an inner diameter of 116 mm and an outer diameter of 124 mm. Two holes at the bottom of the plate allow for insertion of two cylindrical resistance heaters that heat up the substrate to the desired temperature.

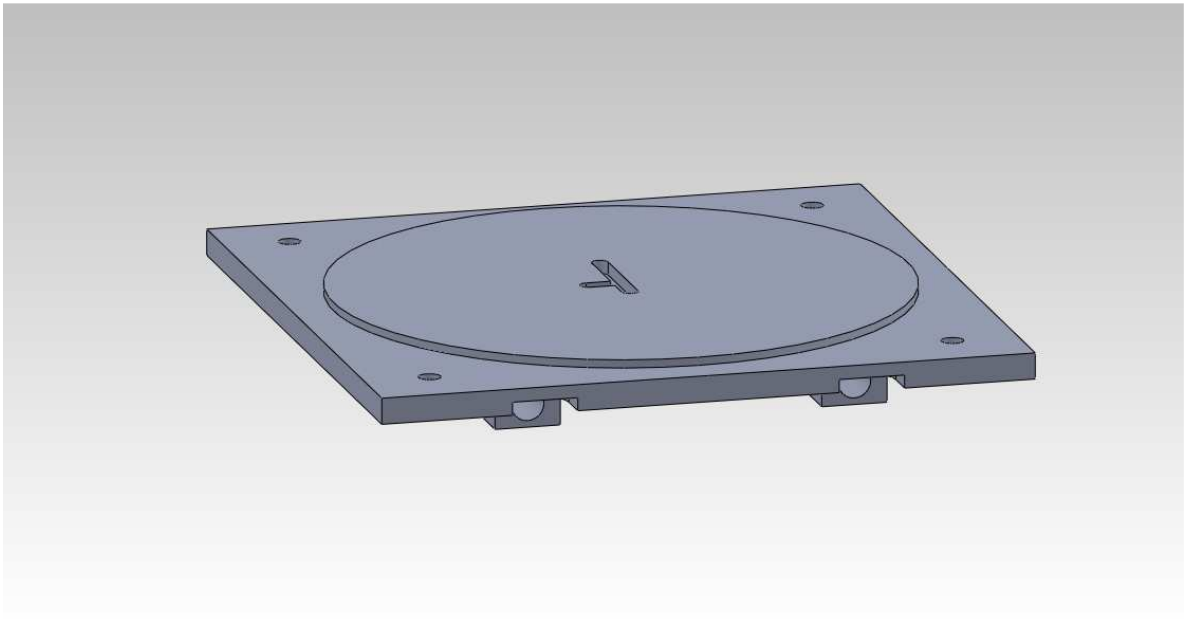

a. Grove for RTDs and heaters

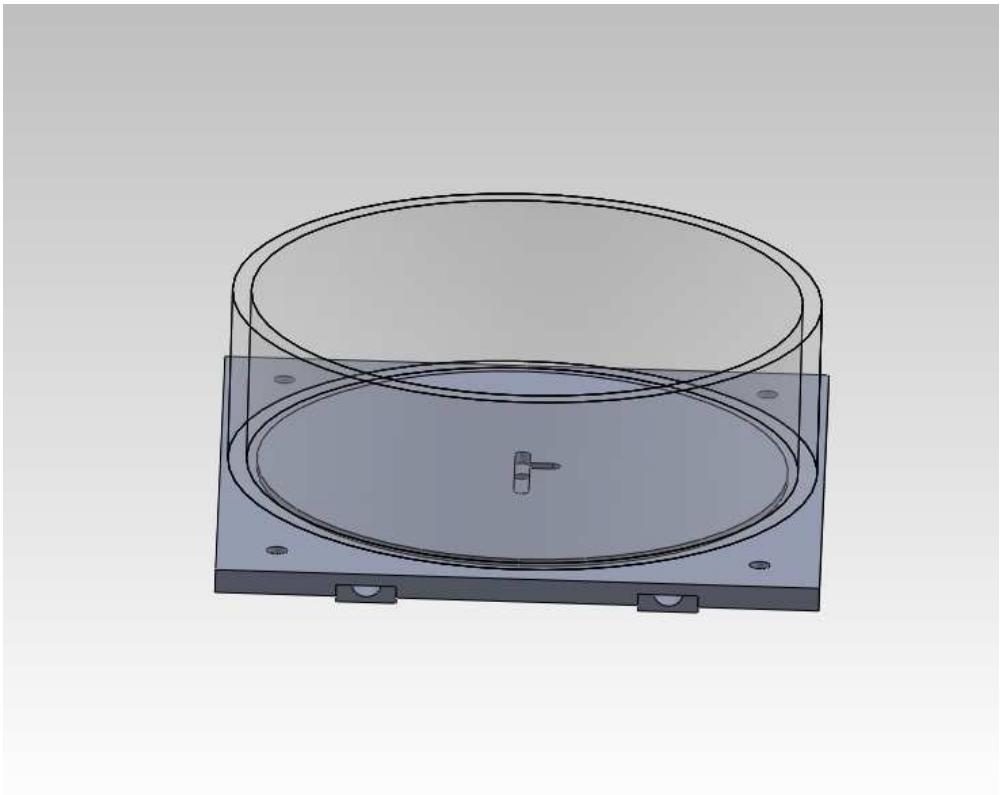

b. Plate and pool wall assembly

Figure 5: Third generation pool design

2.2 Fluid and Thermal Behavior Measurement

A two-pronged approach is used to measure the dynamics of the droplet impacts. A high speed video camera (Phantom v7.1, Vision Research) is used to record the droplet in freefall and the impact cavity from the side parallel to the substrate plane. The camera records at 1000 frames per second at a resolution of 800 x 600 pixels. The exposure time per frame is 40 microseconds. The video is backlit by an LED panel.

Distance and velocity measurements are taken using the Phantom Camera Control software. Video length calibration is done using still frames of objects of known dimensions; from these frames the length corresponding to one pixel on video can be calculated. Measuring the distance a droplet moves between successive frames of video with a known time interval between frames gives the velocity the droplet is moving during that time. The camera is positioned at a height such that the cavity below the surface of the pool is visible as well. Calibration lengths are taken both above and below the surface of the pool to account for refraction. One pixel above the surface of the pool corresponds to 0.030 mm, and below the surface to 0.028 mm.

To provide repeatability, each droplet was assessed before impact. The impact velocity was measured and required to be ±0.05 m/s of the nominal velocity. The droplet diameter was measured both horizontally and vertically in the video plane, and both axes were required to be within ±0.05 mm of each other and of the nominal diameter for the particular needle used. This ensures comparisons between droplets are not subject to variation due to the pre-impact conditions. Further, the shape of the droplet at impact has been observed to greatly influence subsequent cavity, splashing, and vorticity dynamics [8]. Ensuring the droplet is spherical at impact will alleviate these geometry effects.

The second experiment prongs are four fast-response RTDs cast in the epoxy upon the substrate (Omega F-3145). It is advertised with a response time constant of approximately 3 milliseconds. The RTDs are embedded in a T-shaped junction and are exposed but flush with the substrate. The droplet impacts are centered upon the middle

RTD and the rest of the RTDs will pick up the temperatures as the droplet expands and then collapses. The center RTD, R0, is at 0 mm, R1 is 4.81 mm off-center, R2 is 6.57 mm off-center, and R3 is 9.39 mm off-center. The RTDs are sampled at 1000 Hz and the data is digitally smoothed using a moving average filter. They provide detailed and fast-response insight into the heat transfer at the point of impact.

2.3 Thermal Analysis

The RTDs provides records of the temperatures at the substrate. From this, the heat flux is calculated using a numerical integration of Duhamel's theorem. Duhamel's theorem is a method of solving the heat equation for time-fluctuating boundary conditions, enabling the heat flux through a surface to be solved based on a measurement of temperature history [17]. Duhamel's theorem in temperature form, assuming constant thermal properties, is given by Equation 9. T is the temperature, t the time, τ a reference time, and z the vertical coordinate. The substrate temperature response is described by the function T [17].

$$T(z,t) = T_0 + \int_{t_0}^{t} S(z, t-\tau)\frac{dT}{dz}\,dz \tag{9}$$

Modeling the substrate as a solid, semi-infinite plane, S takes the form of Equation *10*.

$$S(z,t) = 1 - \mathrm{erf}\left(\frac{z}{2\sqrt{kt\rho c}}\right) \tag{10}$$

With that response function, and using Fourier's Conduction Law ($q'' = -k\,dT/dz$), Equation 9 can be integrated and solved for the heat flux.

$$q'' = 2\sqrt{\frac{k\rho c}{\pi}}\sum_{i=1}^{I}\frac{T_i - T_{i-1}}{t_i - t_{i-1}}\left(\sqrt{t_I - t_{i-1}} - \sqrt{t_I - t_i}\right) \qquad (11)$$

Where T is the temperature at each time step I, t the time, k, ρ, c, the thermal conductivity, density, and specific heat of the substrate containing the sensor, respectively, and q'' is the heat flux per unit area. The overall heat extraction, q, is calculated by taking the sum of each instantaneous heat flux multiplied by the time step.

This solution assumes a finite time step. Equation 11 is used to estimate the heat flux from the temperature history recorded by the embedded RTDs.

Chapter 3 Results and Discussion

3.1 Scaling of the results

The results were converted to dimensionless values for ease of comparison. A dimensionless characteristic H*, given in Equation 12, was used to characterize the cavity depth. H* is a ratio of the pool height to the droplet diameter.

$$H^* = \frac{H}{d} \qquad (12)$$

With H as the height of the pool and d is the diameter of the droplet.

$$\tau = \frac{t}{t_{capillary}} = \frac{t}{\sqrt{\frac{\rho d^3}{We\sigma}}} \qquad (13)$$

A dimensionless time scale, τ, is defined in Equation 13. $t_{capillary}$ is defined as the time it takes for the capillary wave to develop and collapse. The capillary time can be derived starting from the Weber number as follows:

$$We = \frac{\rho U^2 d}{\sigma} \tag{14}$$

The velocity U from the Weber equation is scaled against the droplet diameter to introduce the capillary timescale Equation 15.

$$U = \frac{d}{t_{capillary}} \tag{15}$$

Combining equations 14 and 15, and solving for the capillary time:

$$t_{capillary} = \sqrt{\frac{\rho d^3}{We\sigma}} \tag{16}$$

For the temperature, a dimensionless characteristic θ, Equation 17 respectively, were used to non-dimensionalize the temperature.

$$\theta = \frac{T - T_d}{T_s - T_d} = \frac{\Delta T_{expected}}{\Delta T_{maximum}} \tag{17}$$

Where T is the final temperature, T_d is the temperature of the droplet, and T_s is the temperature of the substrate.

Finally, a dimensionless δ, shown in Equation 18, was used to characterize the distance of the RTDs from the impact point against the droplet radius.

$$\delta = \frac{l}{r} \tag{18}$$

Here, l is the distance of RTD from impact point and r is the radius of the droplet.

3.2 Single Droplet Cavity Dynamics

Cavity dynamics of single droplet will be discussed as the phenomena relates to the observed behavior of droplet trains. An RTD recorded the temperature history, and the lifetime of the cavity and its depth were visualized using a high speed video camera. The cavity depths were measured in 5 mm, 9 mm, and 15 mm thickness pools at a velocity of 2 m/s. The droplet diameter was fixed at 4.6 mm. The Weber number for these droplets was 270. The still frame images from the video recording corresponding to these pools are shown in Figure 6. The measurements are of the depth of the cavity vertically below the point of impact of the center of the droplet. Figure 7 depicts the cavity depth over time for a droplet impinging upon the different pools. Each of the pool depths produce different qualitative cavity behaviors leading to the categorization of thin-film, intermediate, and deep-pool regimes. In the thin film regime, the solid boundary

dominates the behavior due to contact with substrate whereas in the deep-pool regime, there is minimal to no influence of the solid boundary due to the large separation distance of the drop and substrate. Some influence of the solid boundary is seen with the intermediate regime where the drop approaches the substrate.

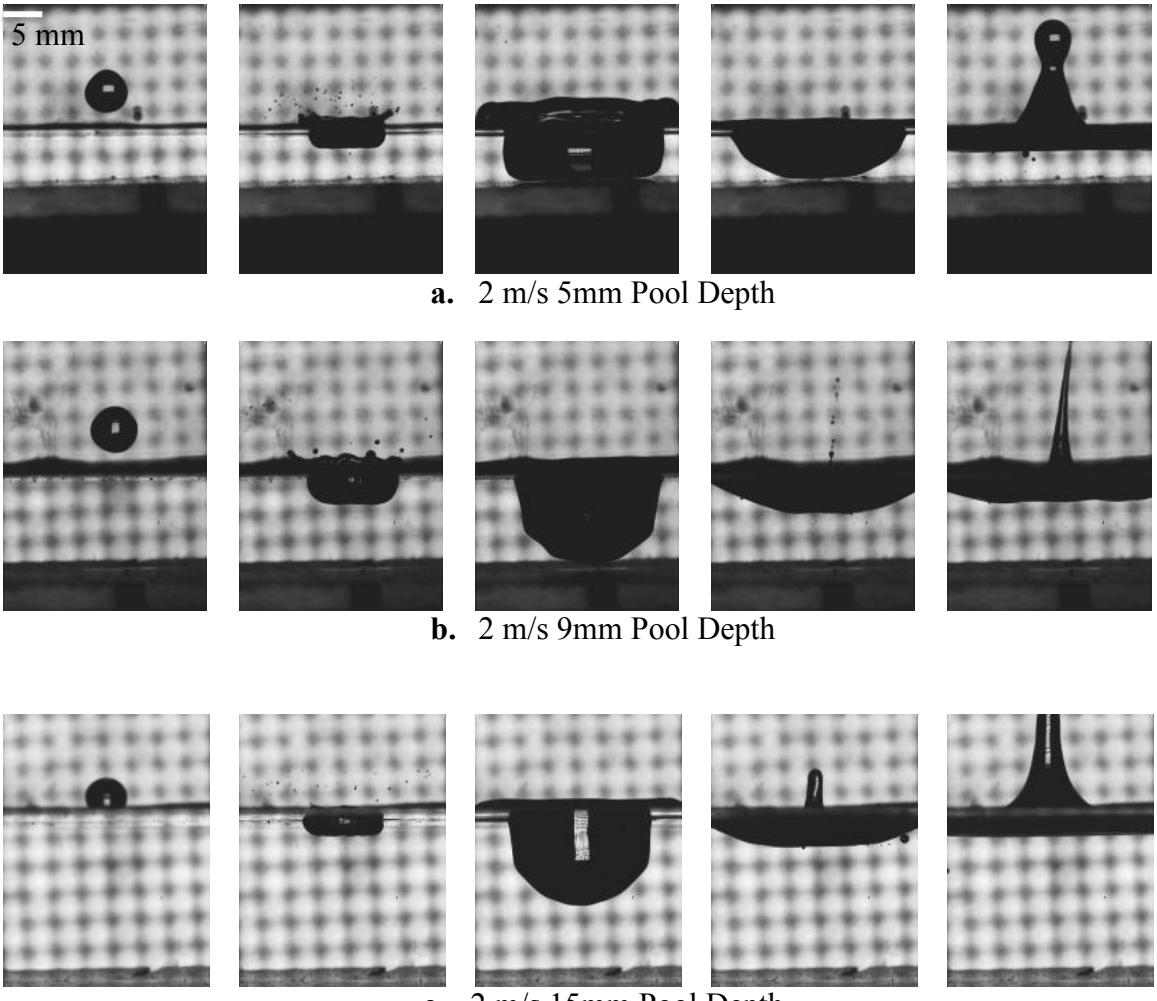

a. 2 m/s 5mm Pool Depth

b. 2 m/s 9mm Pool Depth

c. 2 m/s 15mm Pool Depth

Figure 6: Still frames depicting the cavity formation, at maximum depth, and collapse.

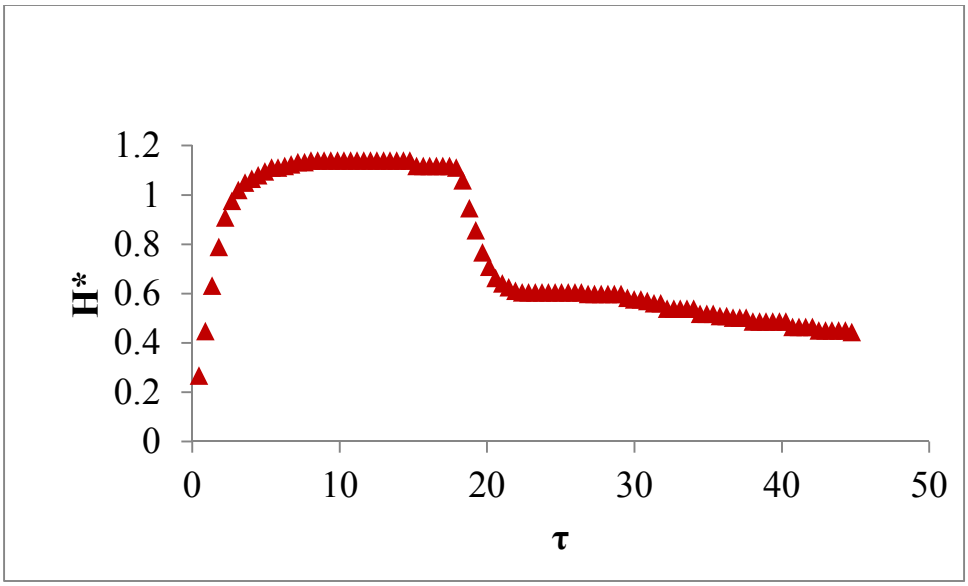

a. 5 mm Pool Depth

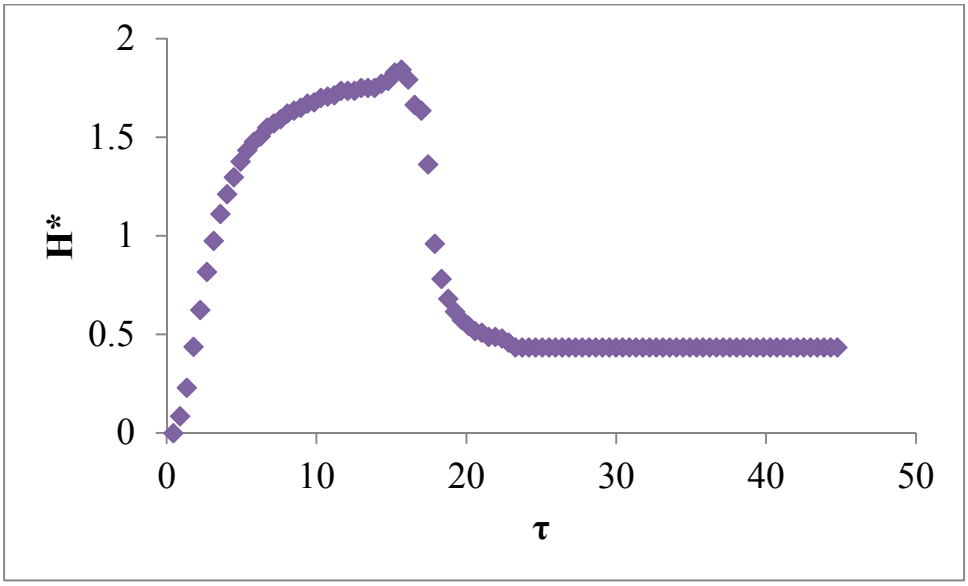

b. 9 mm Pool Depth

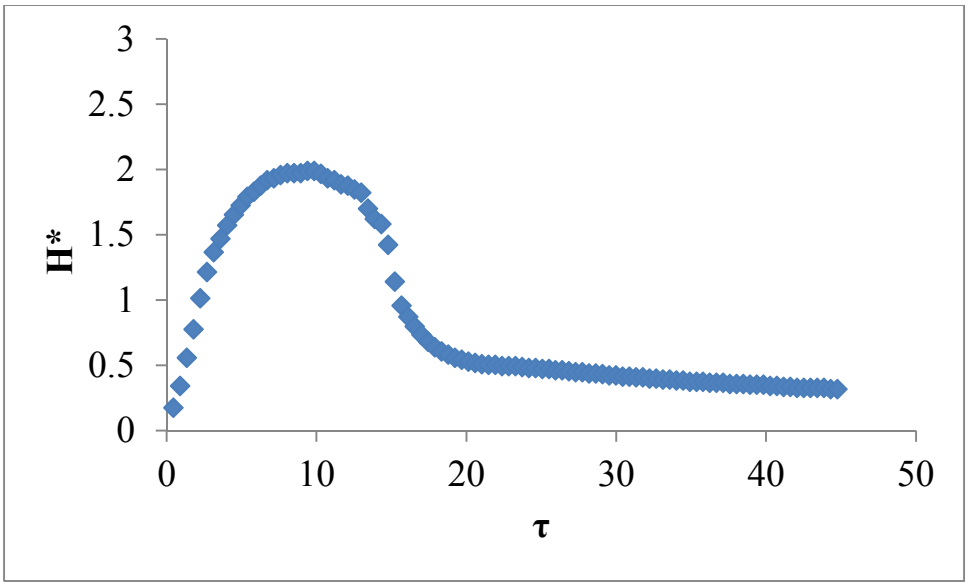

c. 15 mm Pool Depth

Figure 7: Cavity depth temporal evolution within different pool depths

For the 5 mm pool (Figure 6a), the cavity immediately reaches the bottom of the pool causing the pool to act as a thin film. In Figure 7a the cavity can be seen touching the substrate for an extended period of time before rebounding and forming a jet. This can be explained as the momentum of the droplet impact being directed radially outward from the point of impact which leads to an extended period of time when the substrate below the pool is exposed. The quasi-steady cavity condition observed by Trujillo, et al occurred in this regime, as the radial redirection of droplet momentum is what maintains the position of the cavity walls [38].

The deep pool regime is observed when a droplet impacts into the 15 mm pool depth. From Figure 6c it can be seen that the cavity only penetrates halfway into the pool before rebounding and creating a jet. Figure 7c shows the cavity creating a nearly smooth curve as it strains to reach its maximum cavity depth. A small spike is observed before

the pool finally collapses. This spike has previously been discussed by Rein in his 1996 paper where he attributes the radial narrowing of the cavity and the eventual vertical collapse to the absence of a vortex ring due to the high impact Weber number [43]. The absence of the vortex ring causes the flow to be pushed upwards resulting in the observed collapse progression [43].

The 9 mm pool depth displays a cavity that does not appear to be in the thin-film regime nor the deep-pool regime. As seen in Figure 6b, the cavity experiences some interaction with the substrate but less than is seen with the thin-film regime. It also travels significantly nearer to the substrate than the cavity in the deep-pool regime. This substrate interaction can be attributed to viscous effects within the thin layer of fluid that remains between the cavity and the substrate. The cavity, shown in Figure 7b, starts off smooth but is interrupted by a small spike as it reaches its maximum depth. A sharp rebound is observed as the cavity collapses before coming to a rest. Much like the other two pool depths, a jet is formed upon the initial collapse of the cavity before it fully comes to rest.

3.3 Single Droplet Heat Transfer

The temperature history for each of the pool depths is shown in Figure 8. Although the 15 mm cavity did not reach the substrate, it is shown to still have a temperature drop which suggests that some of the droplet fluid traveled through the pool to reach the substrate. This means the droplet fluid distribution differs from the cavity shape and position showing that for some impact and pool conditions, the droplet fluid may be deposited near the substrate as the cavity collapses, for example, leading to an

extended cooling period. From Figure 8 it can be seen that the 9 mm pool depth (the intermediate pool) resulted in the largest temperature difference with an uncertainty of ±0.39 °C whereas the deep pool has the smallest difference between initial and minimum temperature with an uncertainty of ±0.87 °C. Although the droplet liquid did make contact with the substrate, it was then pushed away from the point of measurement leading to a lesser cooling effect at the point of impact than the intermediate pool. While some of the droplet fluid does reach the substrate for the deep-pool regime, the deeper pool does prevent more of the cool fluid from penetrating.

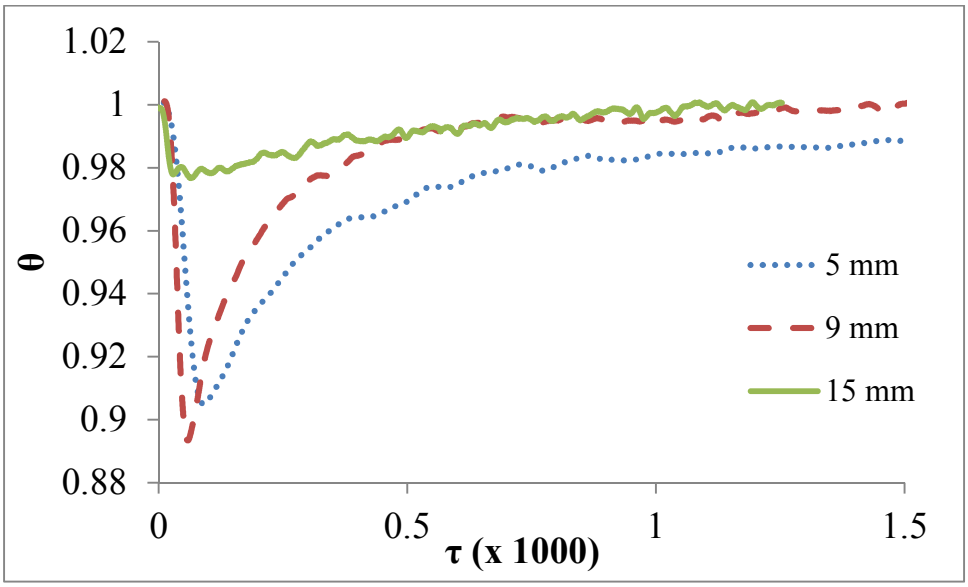

Figure 8: Temperature history for investigated pool depths.

The observation of enhanced cooling for certain pool depths was noted by Vu, et al. [17]. The effect was at that time attributed to a secondary convective phase, produced by eddies of droplet fluid at the substrate after the cavity had collapsed. These eddies are

evidence of droplet fluid deposition at the substrate, as the droplet fluid is left behind and circulated as the cavity recedes. More detail about these vortices is widely available in literature; for now we posit that they are evidence of the findings of cool fluid deposition near the pool substrate complementary to our temperature measurements. Droplet-film impact vortices are well explored, starting from Thomson and Newell in 1885 [44] and continuing through the present. Rein, among others, attributes the penetration of these vortices, composed primarily of droplet fluid, to the droplet's shape at impact- a prolate (along impact axis) drop produces a more powerful and penetrating vortex than an oblate on [43]. Watanabe, et al, discussed these vortices that form around the cavity extensively from the results of their numerical model [45].

If the droplet's impact conditions are such that significant and extended deposition of droplet fluid at the substrate occurs, the cooling effect ought to be larger than cases where the droplet rebounds or otherwise moves away from the substrate. For reference, a droplet impact onto a heated (T_{subs} = 60 °C) dry surface at the same velocity (2 m/s, We = 270) was measured to compare the cooling effects with the impacts onto liquid pools. Figure 9 shows the temperature history for the dry surface impact where the straight line before the initial drop signifies the initial substrate temperature before drop impact and subsequent cooling effects. The temperature drop is significantly larger than any of the pool impact cases and the calculated peak heat flux is 50.6±0.335 W/m^2. The temperature gradually rises but it is not a fast an increase as is seen with the pool. In Figure 10 the droplet is seen impacting the dry substrate, coalescing, and then coming to a rest.

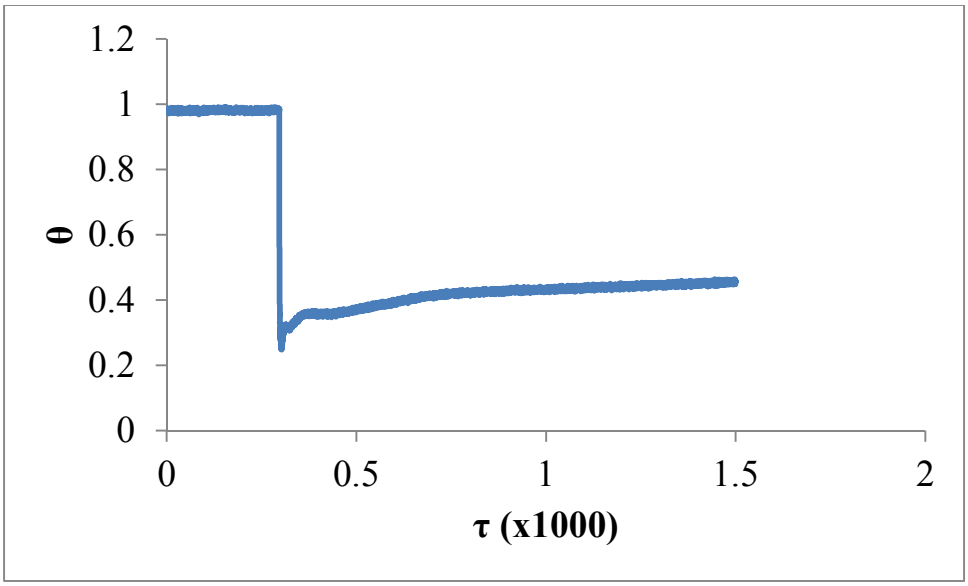

Figure 9: Temperature history for dry substrate

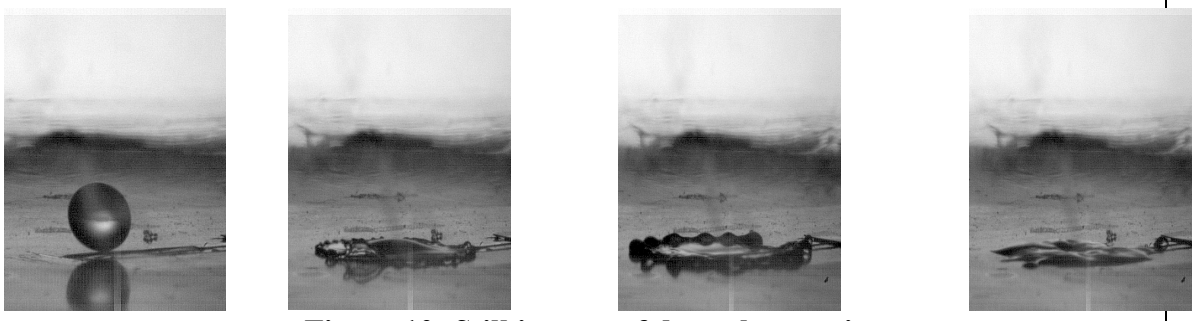

Figure 10: Still images of dry substrate impact

3.4 Droplet Trains Cavity Dynamics

Studying the cavity behavior of single droplets helps better understand the interaction between the cavity and successive droplets in trains of droplets. For instance, in the 5 mm pool, where the thin film regime is observed, the cavity rests at the substrate for an extended period of time. In a train of droplets of sufficient frequency, the next

droplet in the train will fall into the already open cavity. This begins to be seen when the train frequency is approximately 23 Hz. The intermediate and deep-pool cavities collapse slightly more quickly after impact. This necessitates a higher frequency, < 30 Hz, for incoming droplets to impinge upon open cavities. The longer duration in the thin-film regime is likely due to the radial forcing of the droplet momentum, driving the cavity to a larger diameter than the other regimes that delays the closure of the cavity.

Droplet trains lasting 6 seconds were used to explore the thermal effects of trains with varying frequencies. The trains impacted on various pool depths ranging from 4 mm to 15 mm. The trains had constant velocity of 2 m/s. This places the initial impact in the optimal single-droplet cooling regime observed previously. The pool conditions for subsequent droplets are altered by the prior impact. The frequencies used were 0.5, 8, 10, 16, 24, 28, and 32 Hz. Figure 11 shows still frames of successive droplet impacts for each frequency, to explore how exactly the pool conditions are altered for each impact.

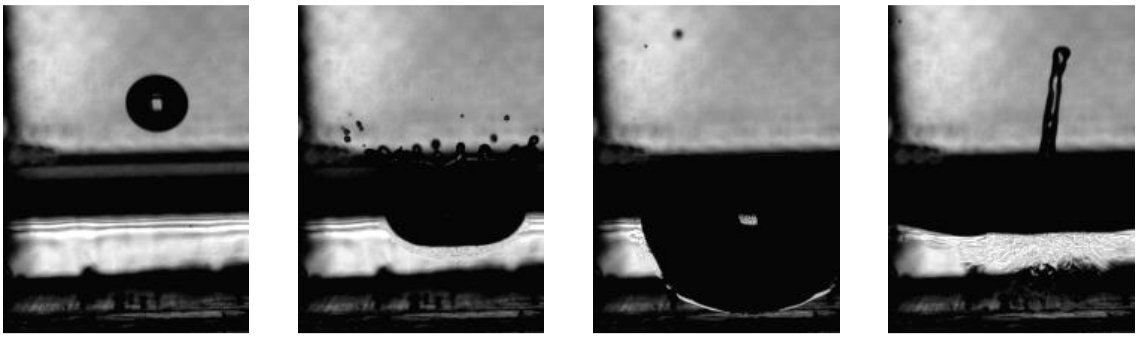

a. 0.5 Hz

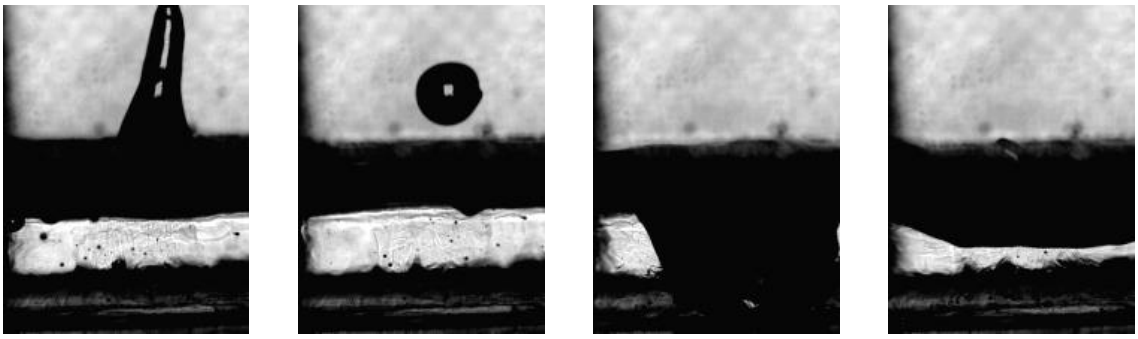

b. 8 Hz

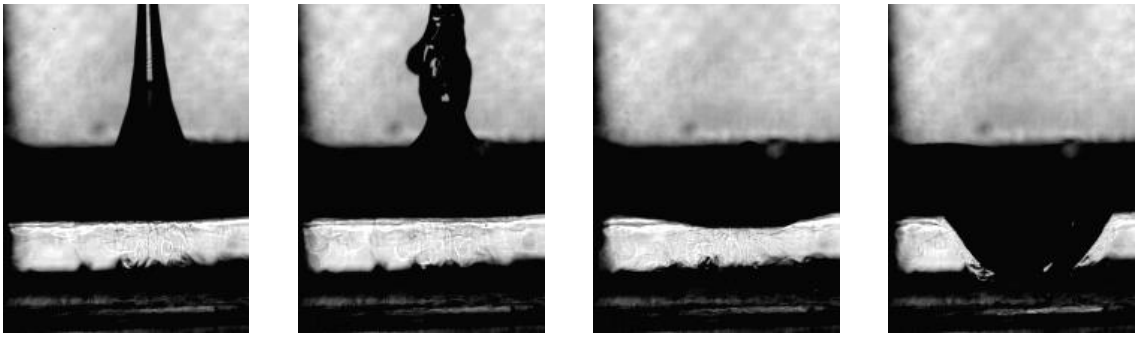

c. 10 Hz

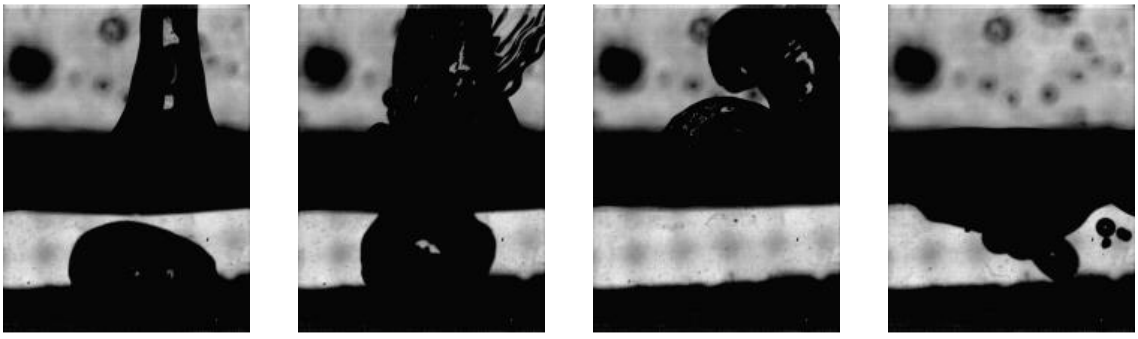

d. 28 Hz

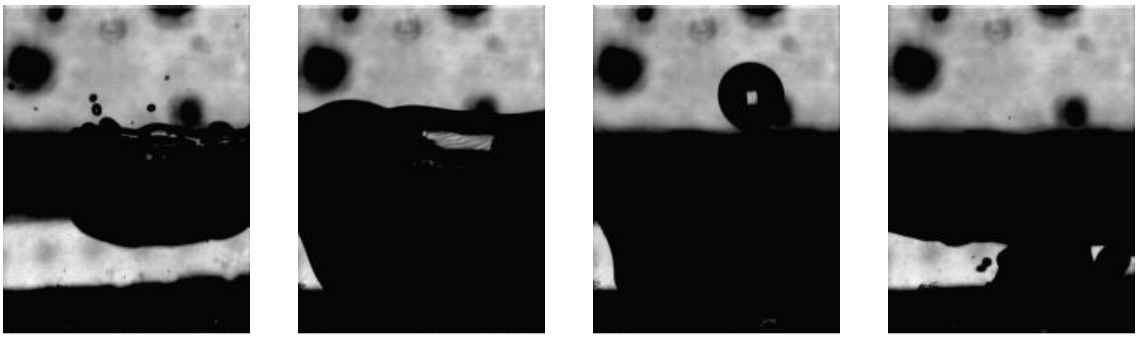

e. 32 Hz

Figure 11: Still frames of successive droplet impacts for each frequency

At 0.5 Hz, successive droplet impacts were nearly isolated from each other- the cavity of one droplet had collapsed and the pool was settling by the time the next droplet arrived (Figure 11a).

At 8 Hz (Figure 11b), the droplets started to show overlap in their impacts. The successive droplets fall into the small cavity created by the previous droplet's jet rebound which allows for better cooling.

At 10 Hz (Figure 11c), the jet from the cavity collapse intercepts the next oncoming droplet causing a delay in cooling which reduces the overall cooling effect.

At 28 Hz (Figure 11d), the cavity dynamics of successive droplets begin to overlap. The pool has not yet become quiescent from one droplet by the time the next has arrived.

At 32 Hz (Figure 11e), each successive droplet impinged within the cavity of the previous, developing towards the quasi-steady cavity condition [38].

3.5 Droplet Trains Heat Transfer

The temperature behavior over time of a 9 mm pool depth was taken for each frequency to understand the cooling behavior as it relates to frequency. Figure 12 shows the temperature history for each frequency.

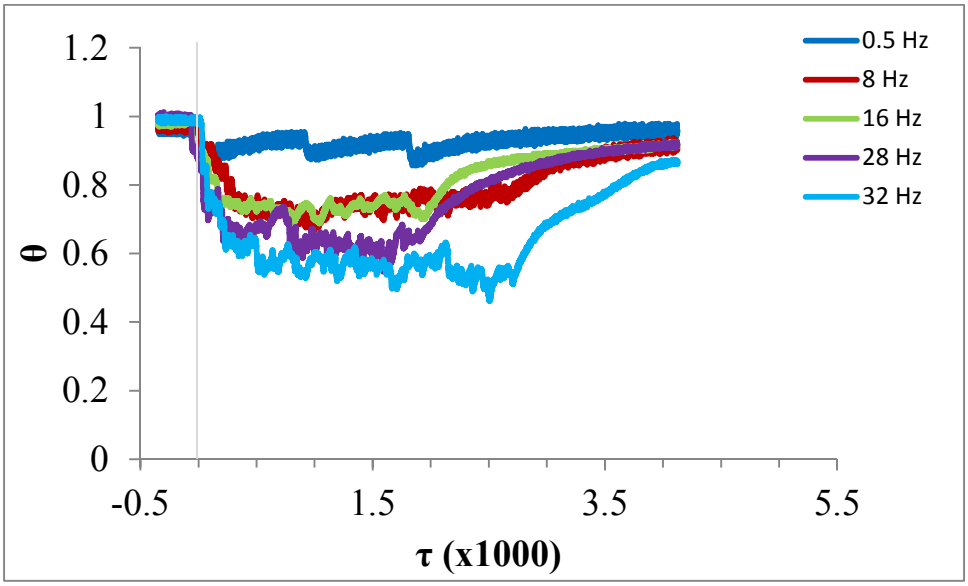

Figure 12: 9 mm temperature history for different frequencies

For the 0.5 Hz, the cooling is largest when compared on a per-droplet basis since each droplet falls after the previous droplet's cooling effects have been settled. Consequently, each successive droplet gives a similar temperature drop, with a sharp initial decrease and smooth minimum. However, the temperature continues to decrease with each successive droplet, giving a cumulative cooling effect.

At 10 Hz, the cooling effects are shown to overlap and jet interference is shown to affect the cooling. As the cooling effects begin to taper off, more droplets fall and some collide with the jet as it is receding causing a change in the cooling.

At 32 Hz, the best cooling effect is observed as the droplets impinge on the cavity created by the previous droplet allowing for better overall cooling. The cavity is left open due to the shorter droplet spacing which allows the next droplet to fall into the cavity and reach the heated substrate. This constant substrate contact allows for the maximum cooling effect which in turn produces the largest overall temperature drop.

The heat flux, Figure 13, appears to follow a sinusoidal trend with regard to frequency. This trend can be attributed to the different stages of jet development at the time of successive droplet impacts. At some frequencies, the jet-droplet collision occurs when the jet is still developing leading to a slowed droplet which produces a lower heat flux. At other times, the jet-droplet collision occurs as the jet is collapsing and the collapse pulls the droplet into the pool resulting in a higher heat flux. Heat flux measurement was taken for a 36 mm deep pool to show that at a deep enough pool, the cooling effects can be deemed negligible.

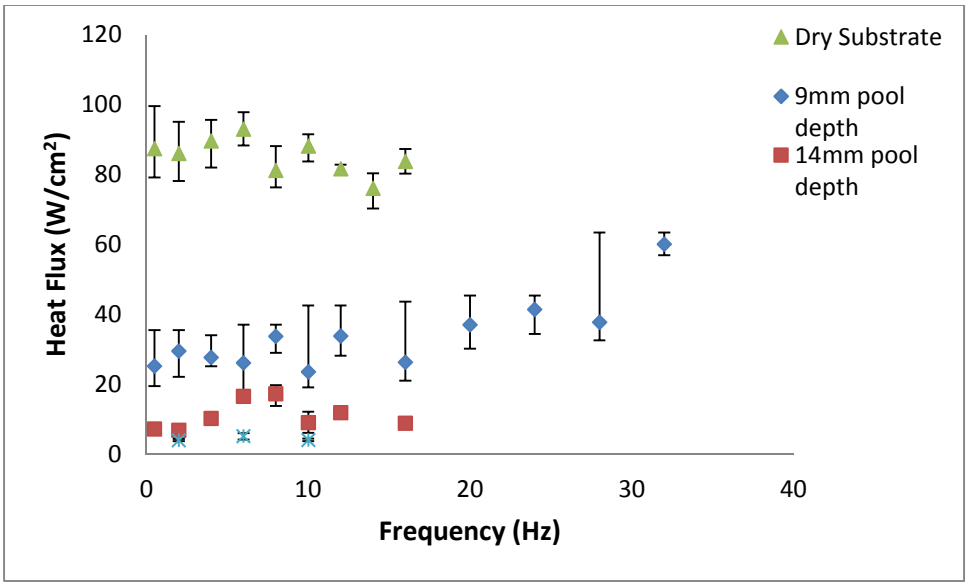

Figure 13: Peak heat flux for different frequencies

Dry surface cooling effect was also studied using the different frequencies mentioned above. It can be seen from Figure 13 that the dry surface produces higher heat flux than that produced when droplets impinge into a pool. As the frequency increases, the peak heat flux produced becomes smaller and this can be attributed to the buildup of a thin film layer caused by the higher number of droplets released at that frequency. Figure 14 shows the temperature measurements from some of the frequencies used.

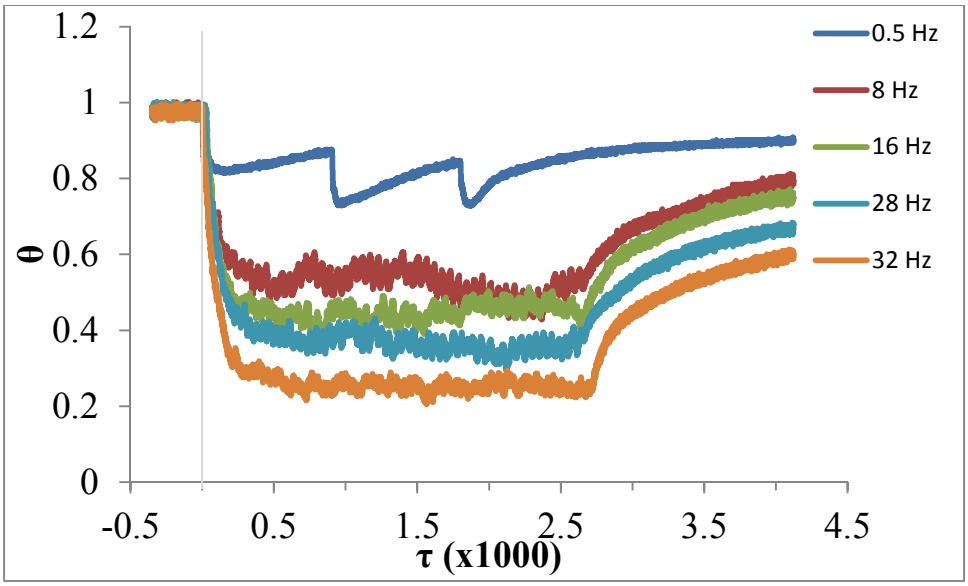

a. 32 Hz

Figure 14: Temperature history for dry surface with different frequencies

At 0.5 Hz , there is a clear distinction between each temperature fluctuation due to the next drop impinging after the previous drop had begun warming up. This means that individually, each droplet produced larger temperature difference than the other drops of higher frequencies but the cumulative cooling was severely reduced due to the large spacing. This large spacing experienced by the 0.5 Hz is shown to be reduced for the 8 Hz leading to better cumulative cooling.

As the frequency increased, the spacing was reduced leading up to the 32 Hz where the spacing is almost indecipherable. The 32 Hz frequency shows the largest overall difference in temperature since the drops were so closely spaced that each drop impinged before the previous droplet could rise back to the original temperature of the heated substrate.

For the frequencies studied, the most effective cooling in terms of heat flux occurs as the frequency increases. The cooling period of each droplet at higher frequency overlaps with the next, leading to a cumulative high heat flux.

Multiple RTDs were used to measure the temperature history as the droplet expanded then collapsed. The RTDs were placed such that one would record the immediate impact temperature and the rest will record the temperatures as the drops expanded (Figure 15). R0, which is the center RTD, is at 0 mm, R1 is 4.81 mm off-center, R2 is 6.57 mm off-center, and R3 is 9.39 mm off-center. Figure 16 shows the temperature measurements for each of the frequencies used for the 9 mm pool depth. Figure 17 shows the temperature measurements for the dry substrate.

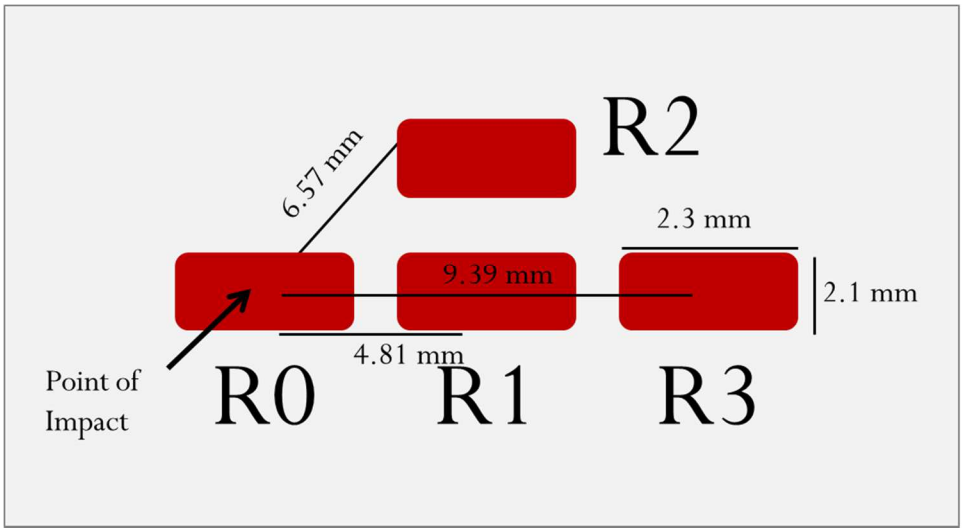

Figure 15: RTD placement

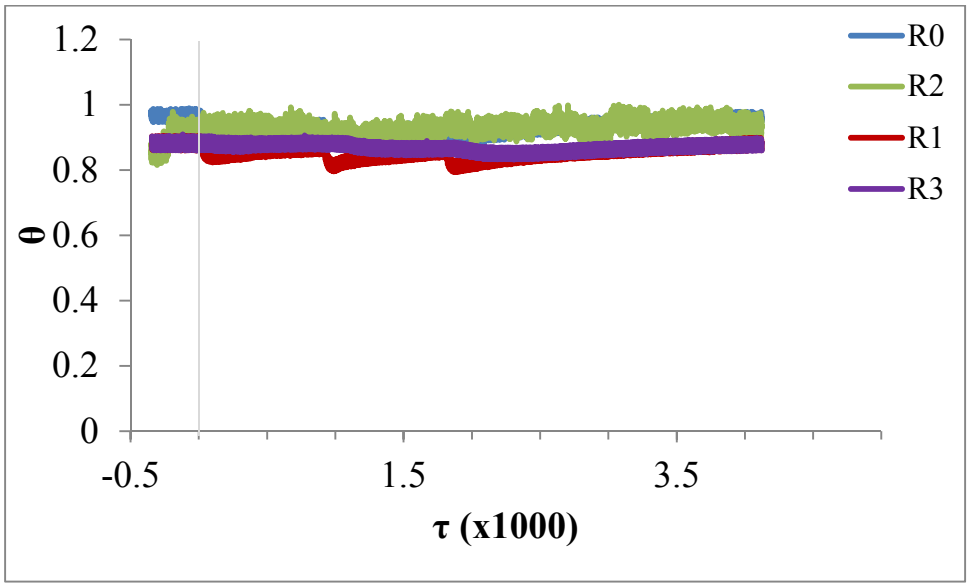
1.2
1
0.8
θ 0.6
0.4
0.2
0
-0.5
1.5
3.5
τ (x1000)
R0
R2
R1
R3

a. 5 Hz

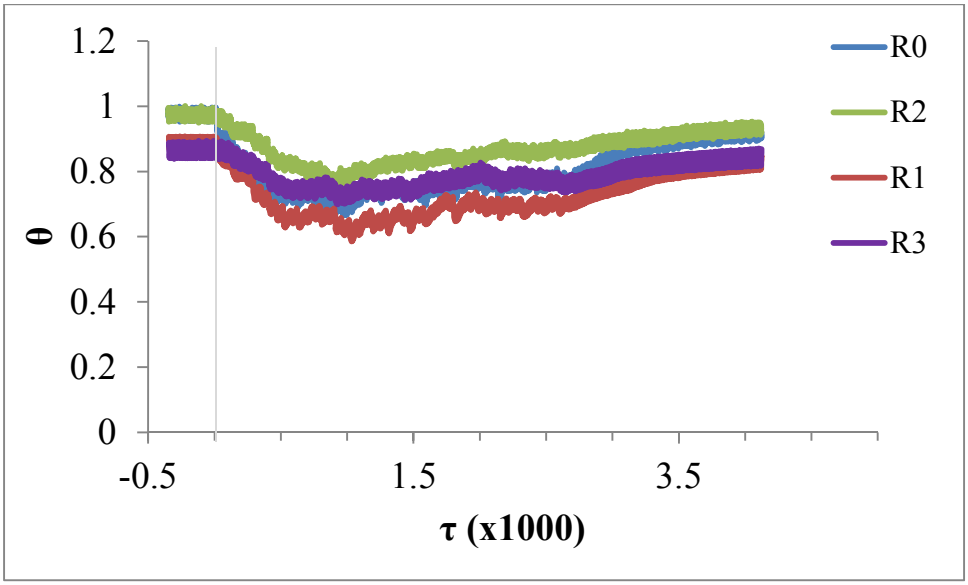
1.2
1
0.8
θ 0.6
0.4
0.2
0
-0.5
1.5
3.5
τ (x1000)
R0
R2
R1
R3

b. 8 Hz

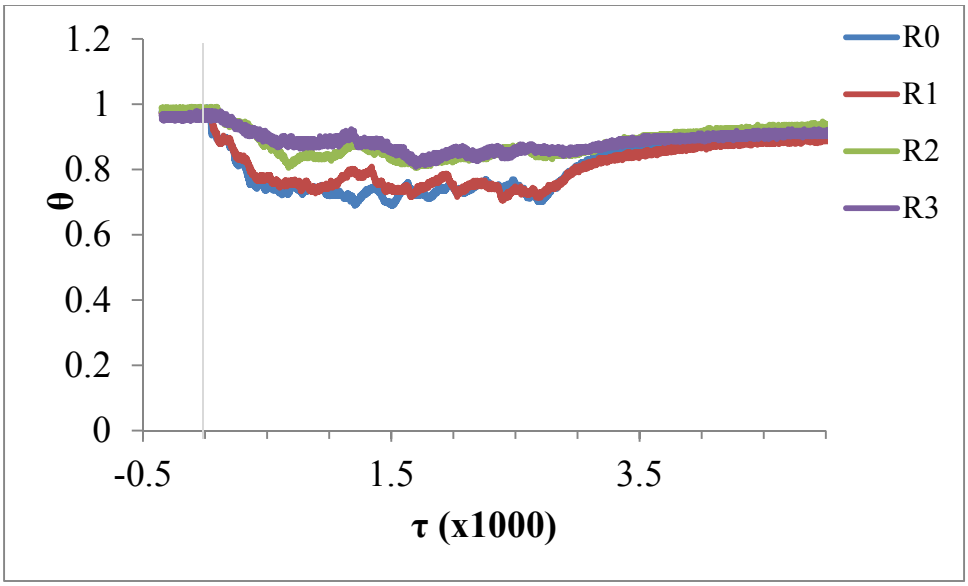
1.2
1
0.8
0.6
0.4
0.2
0
θ
-0.5
1.5
3.5
τ (x1000)
R0
R1
R2
R3

c. 16 Hz

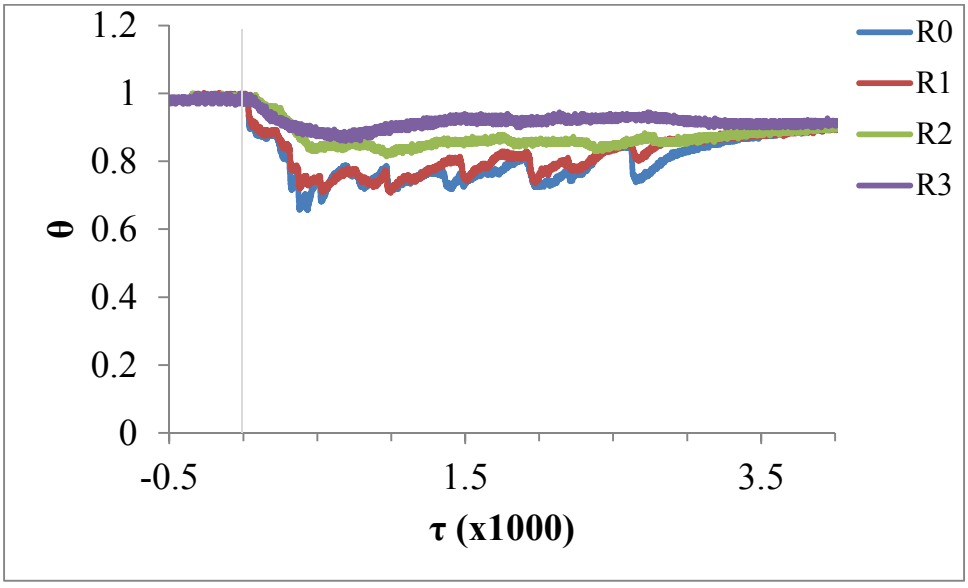
1.2
1
0.8
0.6
0.4
0.2
0
θ
-0.5
1.5
3.5
τ (x1000)
R0
R1
R2
R3

d. 24 Hz

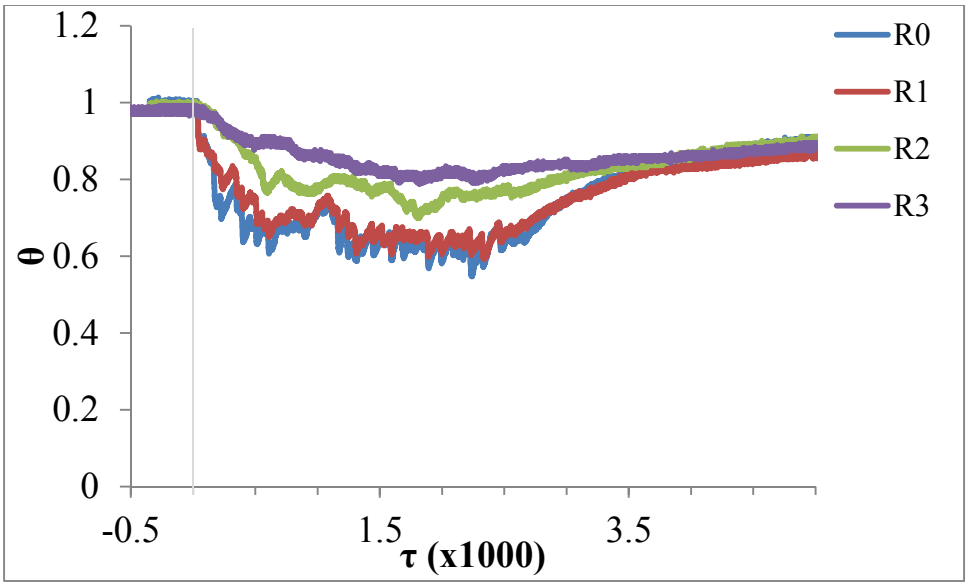

e. 28 Hz

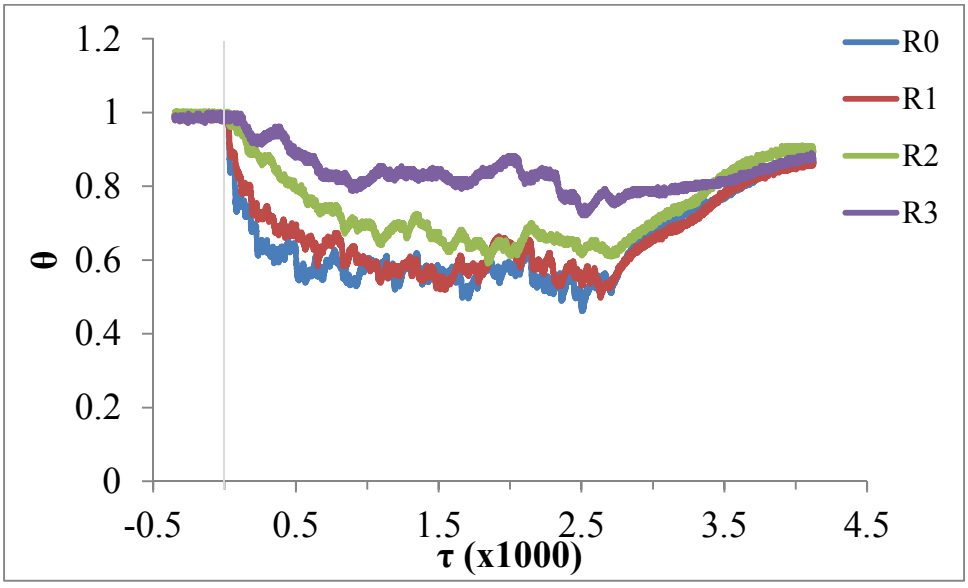

f. 32 Hz

Figure 16: 9 mm pool temperature measurements using multiple RTDs

At 5 Hz (16a), R1 served as the point of impact with the droplet missing the intended R0. The droplet separation is evident for all the RTDs with the exception of R3

where there is no clear distinction of temperature change. This could be explained as the droplet subsequent droplets not reaching that RTD thereby causing it to retain the temperature of the first impact. R1 also served as an impact point for the 8 Hz (16b) frequency leading that RTD to produce the largest temperature difference.

At 16 -32 Hz (16c-f), the droplets hit the intended impact point (R0) which resulted in R0 consistently producing the largest temperature difference. 32 Hz frequency (16f) provided the largest temperature difference owing it to the larger amount of liquid continuously impinging onto the open crater and making contact with the impact point. R3 RTD consistently produced the lowest temperature drop due to its distance from the impact point. Since it is the farthest away from the impact point, the fluid will have begun to rise in temperature before the reaching that RTD. However, the continuous onslaughts of droplets were also able to push fluids to the outer regions causing the R3 of the 32 Hz frequency to produce a significantly larger temperature drop than the rest of the R3 from other frequencies.

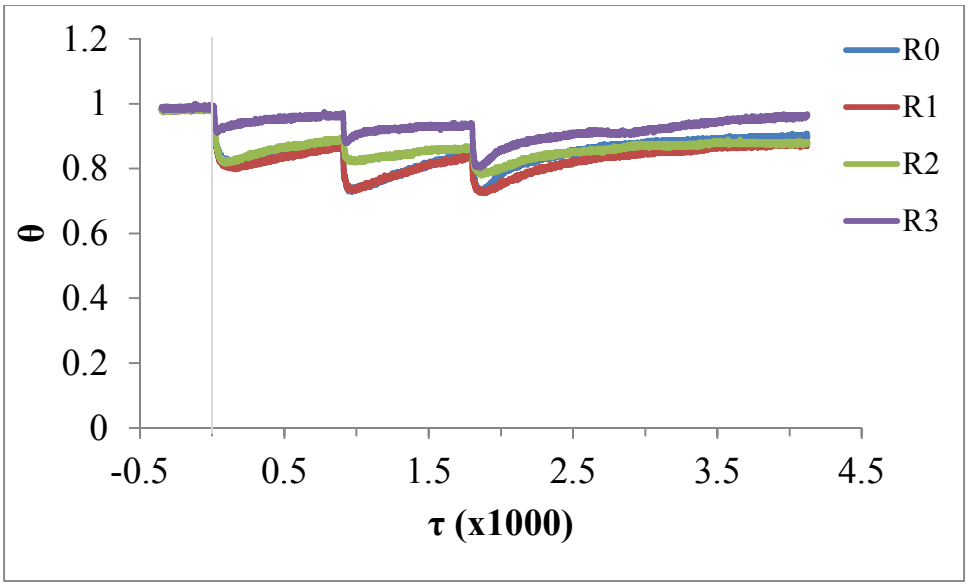
1.2
1
0.8
0.6
0.4
0.2
0
θ
-0.5
0.5
1.5
2.5
3.5
4.5
τ (x1000)
R0
R1
R2
R3

a. 0.5 Hz

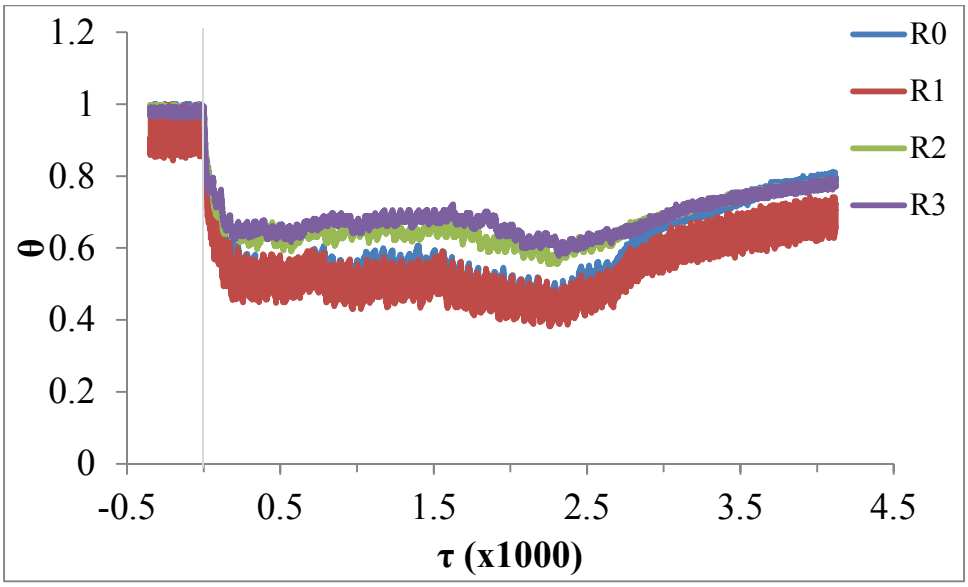
1.2
1
0.8
0.6
0.4
0.2
0
θ
-0.5
0.5
1.5
2.5
3.5
4.5
τ (x1000)
R0
R1
R2
R3

b. 8 Hz

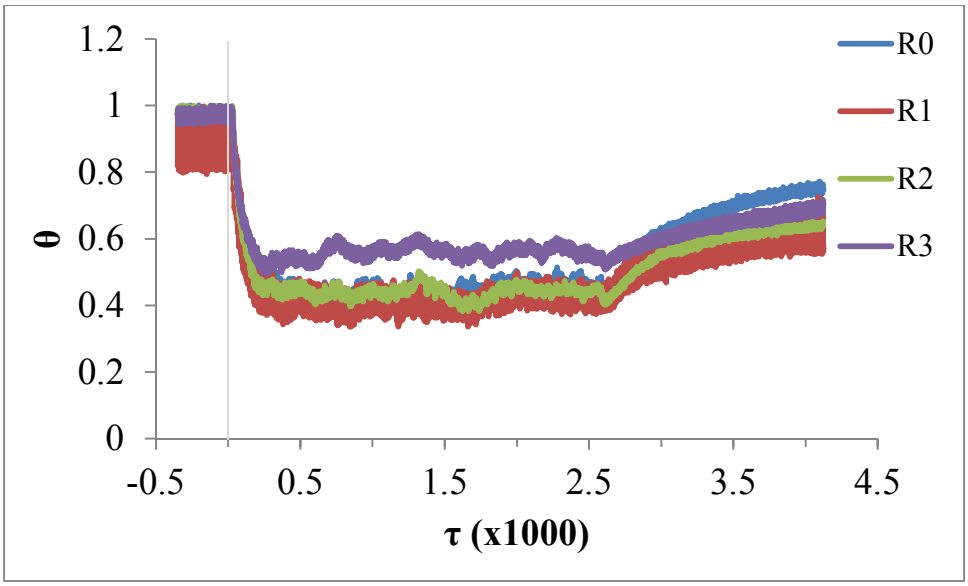
1.2
1
0.8
0.6
0.4
0.2
0
θ
-0.5
0.5
1.5
2.5
3.5
4.5
τ (x1000)
R0
R1
R2
R3

c. 16 Hz

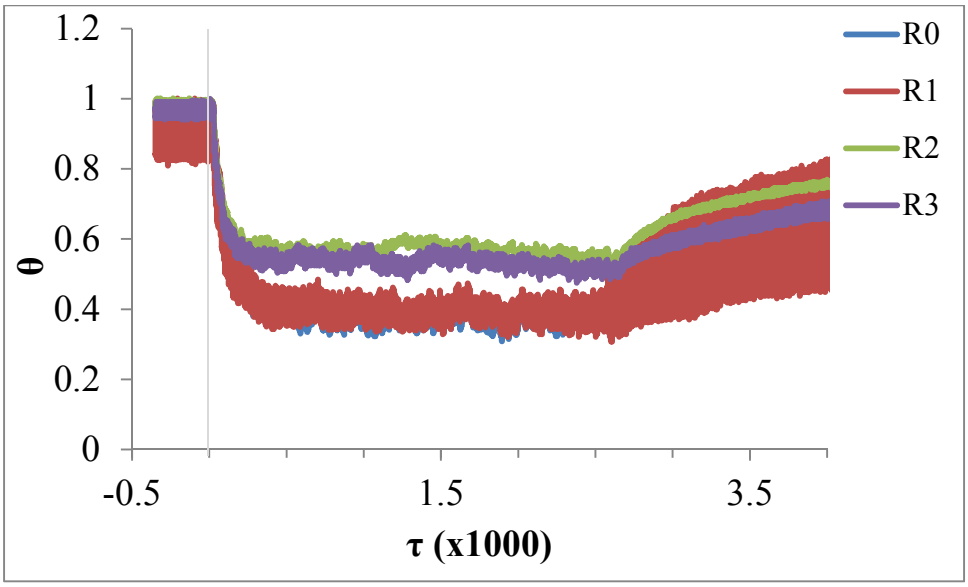
1.2
1
0.8
0.6
0.4
0.2
0
θ
-0.5
1.5
3.5
τ (x1000)
R0
R1
R2
R3

d. 24 Hz

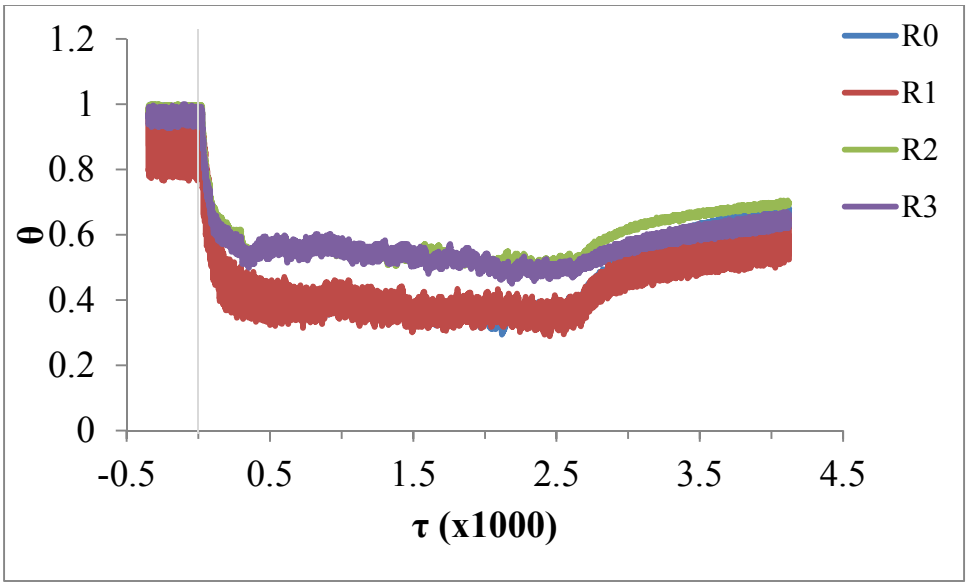

e. 28 Hz

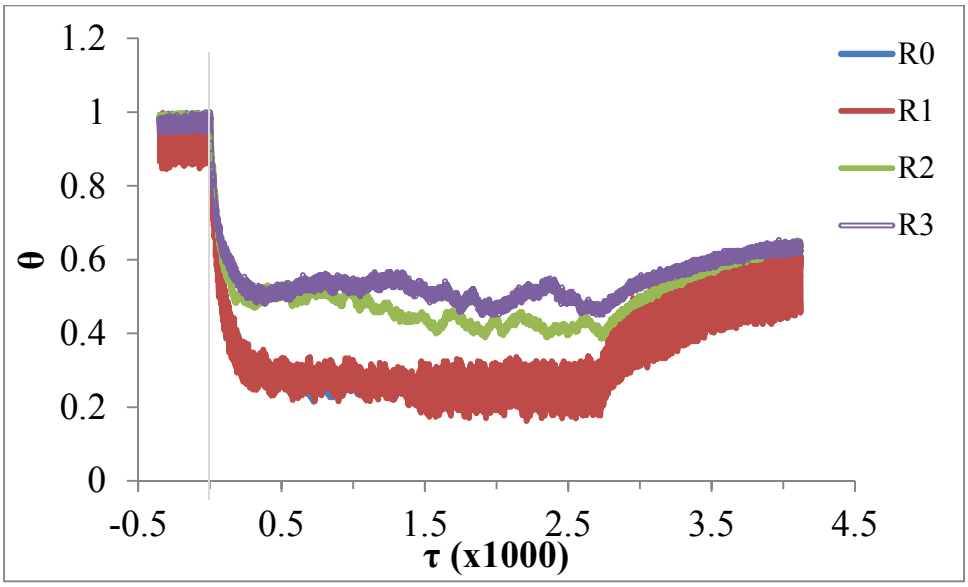

f. 32 Hz

Figure 17: Dry substrate temperature measurements using multiple RTDs

From the plots of droplet train impingement unto dry substrate, it can be seen that there is decrease in cooling the farther the droplet moved away from the impact point. R0 was shown to have the highest temperature difference for most of the frequencies with the exception of a few where the droplet impacted off-center. R3, which was the farthest

away at a distance of 9.39 mm, consistently produced the lowest temperature difference with the exception of 24 Hz (Figure 17d) frequency where R2 produced the lowest. This could potentially be attributed to an unusual deformation of the droplets where the warmer liquid was pushed towards the R2.

At 0.5 Hz (Figure 17a), the first droplet impacted off center hitting R2 which resulted in a higher cooling for that RTD and lesser cooling for the center RTD, R0. The cooling effects of the subsequent drops are reduced due to the pre-wetting of the surface by the initial drop. The RTD at point 4 (R3) continues to exhibit the lowest cooling due to its distance from the rest of the RTDs.

At 16 Hz (Figure 17c), the droplets did not impinge at R0 but instead at R2 causing R2 to have the largest temperature decrease. The droplets spread outward first reaching the R0 with cooler liquid before reaching the rest of the RTDs causing cooling that is not as effective as the R2 and R0.

For the 32 Hz (Figure 17f), the R0 and R1 RTD readings are relatively close in the amount of temperature decrease. As expected, the farthest RTD produced the lowest temperature due to the farther distance the liquid had to travel which caused some heating along the way.

Finally, minimum temperature difference measurements were done for the 9 mm pool depth (Figure 18) and the dry substrate (Figure 19) in comparison to the distance of the RTD from the impact point. The two plots help emphasize the decrease in temperature as the droplets move away from the impact point.

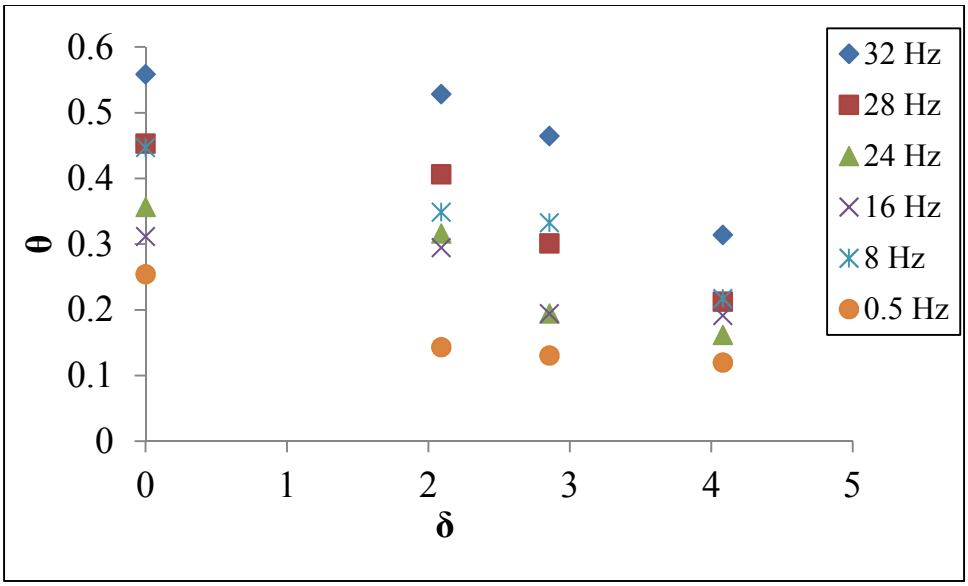

Figure 18: 9 mm pool depth temperature decrease against distance

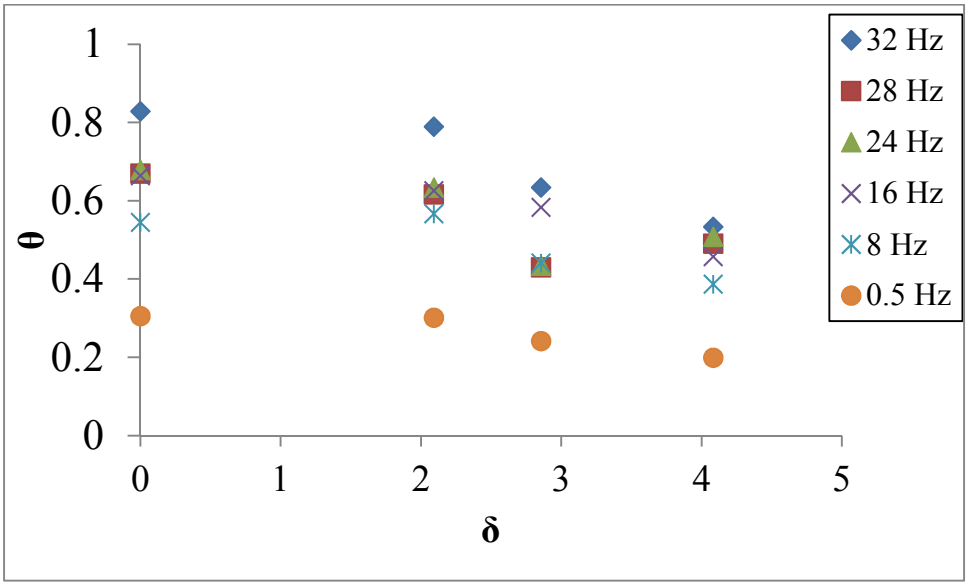

Figure 19: Dry substrate temperature decrease against distance

Chapter 4 Conclusion

The main purpose of this study was to investigate the heat transfer and droplet train dynamics to better understand spray cooling. This was done by studying and characterizing single droplet and droplet train cavity dynamics as well as the heat transfer of varying surface conditions.

This study found for single droplet impact, the presence of the liquid pool reduces the effective cooling at and near the point of droplet impact. For spray cooling applications where the highest heat flux is needed, the liquid delivered by the spray should be minimized to prevent the buildup of the liquid film on the surface. This is one situation where phase change heat transfer that is often present in spray cooling applications, although not investigated in this study, would be highly beneficial. Evaporation is often accompanied by increased heat flux over convection alone, and it further acts to remove liquid from the sprayed area – a dual effect that should serve to prevent film buildup and maximize the spray's cooling effects.

In cases where a large buildup of a liquid pool is unavoidable, a higher impact frequency should be implemented to not only allow the fluid to penetrate the intended points through the open cavity created by previous impacting droplets and to also avoid interference of developing jets. The ideal cooling configuration where a film is present on the substrate is a spray that produces the quasi-steady cavity condition, allowing incoming droplets to reach the substrate as easily as possible.

Higher impact frequencies in dry surface situations will help minimize the development of the thermal boundary layer, which occurs as the droplet spreads out over larger areas, due to the constant influx of cold liquid pushing heated liquid out of the way. Heat flux findings from the droplet trains are in good agreement with Soriano, et al.'s [39] finding. This good agreement shows that high heat fluxes can be obtained with larger droplets (mm sized) and smaller frequencies (in the tens).

Chapter 5 Future Work

Exploring other liquids such as different aqueous mixtures of glycerol, FC-72, ethanol, etc. will allow for comparison to determine the influence of liquid properties on cooling effects. Various velocities for the droplets free-falling into the pool will also be investigated to obtain the optimal velocity required for cooling. Changing the surface conditions of the substrate will be explored. Hydrophobic and hydrophilic conditions will be achieved through the nano/micro-patterning of the surfaces. Alternatively, the surface conditions can also be achieved through laser patterning of the surface. Changing the surface conditions will help in cleaning applications. For example, the hydrophobicity condition can be used in applications where corrosion is not desired such as turbine cooling.

Expanding the range of train frequencies, using multiple axis trains (i.e., offset radially from the first droplet's impact point), and varying the droplet size is another step to build from this study. Existing studies on droplet trains have typically used much smaller (often micron-scale) droplets at much higher frequencies (O(kHz)) [38]; the gap between this study and those conditions is worth closing. Using multiple nozzles to

generate droplets and changing the droplet generator to achieve more droplets with each run will allow for the connection between individual droplets and sprays.

References

[1] Pautsch, A.G., & Shedd, T.A. (2005). Spray impingement cooling with single- and multiple-nozzle arrays. Part I: Heat transfer data using FC-72. *International Journal of Heat and Mass Transfer*, 48(15) 3167-3175

[2] Zhang, H.Y., Pinjala, D., Wong, T.N., Toh, K.C, & Yoshi, Y.K. (2005). Single-phase liquid cooled microchannel heat sink for electronic packages. *Applied Thermal Engineering,* 25, 1472-1487

[3] Imura, H., Kusuda, H., Ogata, J.I., Miyazaki, T., & Sakamoto, N. (1979). Heat transfer in two phase closed-type thermosyphons. *Heat Transfer Japanese Research*, 8, 41-53

[4] Heindel, T.J., Ramadhyani, S., & Incropera, F.P. (1992). Liquid Immersion Cooling of a Longitudinal Array of Discrete Heat Sources in Protruding Substrates: II—Forced Convection Boiling. *Journal of Electronics Packaging*, 114, 63-70

[5] Glynn, C., O'Donovan, T., & Murray, D. B. (2005). Jet impingement cooling. In *Proceedings of the 9th UK National Heat Transfer Conference, Manchester, England,* 5-6

[6] Wang, Y., & Vafai, K. (2000). An experimental investigation of the thermal performance of an asymmetrical flat plate heat pipe. *International Journal of Heat and Mass Transfer*, *43*(15), 2657-2668

[7] Kim, J. (2007). Spray cooling heat transfer: The state of the art. *International Journal of Heat and Fluid Flow*, 28, 753–767

[8] Mudawar, I. (2001). Assessment of high-heat-flux thermal management schemes. *Components and Packaging Technologies, IEEE Transactions on*, *24*(2), 122-141

[9] Shedd, T. A. (2007). Next generation spray cooling: high heat flux management in compact spaces. *Heat Transfer Engineering*, *28*(2), 87-92

[10] Aguilar, G., Díaz, S. H., Lavernia, E. J., & Nelson, J. S. (2002). Cryogen spray cooling efficiency: Improvement of port wine stain laser therapy through multiple-intermittent cryogen spurts and laser pulses. *Lasers in surgery and medicine*, *31*(1), 27-35

[11] Aguilar, G., Wang, G. X., & Nelson, J. S. (2003). Effect of spurt duration on the heat transfer dynamics during cryogen spray cooling. *Physics in Medicine and Biology*, *48*(14), 2169

[12] Aguilar, G., Franco, W., Liu, J., Svaasand, L. O., & Nelson, J. S. (2005). Effects of hypobaric pressure on human skin: implications for cryogen spray cooling (part II). *Lasers in surgery and medicine*, *36*(2), 130-135

[13] Kim, S. C., & Ryou, H. S. (2003). An experimental and numerical study on fire suppression using a water mist in an enclosure. *Building and Environment*, *38*(11), 1309-1316

[14] Arcoumanis, C., & Chang, J. C. (1993). Heat transfer between a heated plate and an impinging transient diesel spray. *Experiments in Fluids*, *16*(2), 105-119

[15] Pais, M.R., Chow, L. C., & Maheikey, E. T. (1992). Surface roughness and its effects on the heat transfer mechanism in spray cooling. *Journal of Heat Transfer*, *114*, 211

[16] Banks, D., Ajawara, C., Sanchez, R., Surti, H., & Aguilar, G. (2013). Effects of drop and film viscosity on drop impacts onto thin films. *Atomization and Sprays*, *23*(6), 525-540

[17] Vu, H., Aguilar, G., & Jepsen, R. (2009). Single droplet heat transfer through shallow liquid pools. In *International Conference on Liquid Atomization and Spray Studies. Vail, CO*.

[18] Worthington, A. M. (1882). On impact with a liquid surface. *Proceedings of the Royal Society of London*, *34*(220-223), 217-230

[19] Worthington, A. M., & Cole, R. S. (1897). Impact with a liquid surface, studied by the aid of instantaneous photography. *Philosophical Transactions of the Royal Society of London. Series A, Containing Papers of a Mathematical or Physical Character*, 137-148

[20] Allen, R. F. (1975). The role of surface tension in splashing. *Journal of colloid and interface science*, *51*(2), 350-351

[21] Rein, M. (1993). Phenomena of liquid drop impact on solid and liquid surfaces.*Fluid Dynamics Research*, *12*(2), 61

[22] Wang, A. B., & Chen, C. C. (2000). Splashing impact of a single drop onto very thin liquid films. *Physics of Fluids (1994-present)*, *12*(9), 2155-2158

[23] Yarin, A. L., & Weiss, D. A. (1995). Impact of drops on solid surfaces: self-similar capillary waves, and splashing as a new type of kinematic discontinuity.*Journal of Fluid Mechanics*, *283*, 141-173

[24] Tropea, C., & Marengo, M. (1999). The impact of drops on walls and films.*Multiphase Science and Technology*, *11*(1)

[25] Yarin, A. L. (2006). Drop impact dynamics: splashing, spreading, receding, bouncing…. *Annu. Rev. Fluid Mech.*, *38*, 159-192

[26] Huang, Q., & Zhang, H. (2008). A study of different fluid droplets impacting on a liquid film. *Petroleum science*, *5*(1), 62-66

[27] Banks, D., Ajawara, C., Sanchez, R., Surti, H., & Aguilar, G. (2014). EFFECTS OF LIQUID AND SURFACE CHARACTERISTICS ON OSCILLATION BEHAVIOR OF DROPLETS UPON IMPACT. *Atomization and Sprays*, *24*(10)

[28] Weiss, D. A., & Yarin, A. L. (1999). Single drop impact onto liquid films: neck distortion, jetting, tiny bubble entrainment, and crown formation. *Journal of Fluid Mechanics*, *385*, 229-254

[29] Bussmann, M., Chandra, S., & Mostaghimi, J. (2000). Modeling the splash of a droplet impacting a solid surface. *Physics of Fluids, 12*(12), 3121-3132

[30] Trujillo, M. F., & Lee, C. F. (2001). Modeling crown formation due to the splashing of a droplet. *Physics of Fluids (1994-present)*, *13*(9), 2503-2516

[31] Fedorchenko, A. I., & Wang, A. B. (2004). On some common features of drop impact on liquid surfaces. *Physics of Fluids (1994-present)*, *16*(5), 1349-1365

[32] Liu, J., Vu, H., Yoon, S. S., Jepsen, R. A., & Aguilar, G. (2010). Splashing phenomena during liquid droplet impact. *Atomization and Sprays*, *20*(4)

[33] Liang, G., Guo, Y., Shen, S., & Yang, Y. (2014). Crown behavior and bubble entrainment during a drop impact on a liquid film. *Theoretical and Computational Fluid Dynamics*, *28*(2), 159-170

[34] Senda, J., Yamada, K., Fujimoto, H., & Miki, H. (1988). The heat-transfer characteristics of a small droplet impinging upon a hot surface. *JSME international journal. Ser. 2, Fluids engineering, heat transfer, power, combustion, thermophysical properties*, *31*(1), 105-111

[35] Di Marzo, M., Tartarini, P., Liao, Y., Evans, D., & Baum, H. (1993). Evaporative cooling due to a gently deposited droplet. *International Journal of Heat and Mass Transfer*, *36*(17), 4133-4139

[36] Aguilar, G., Majaron, B., Verkruysse, W., Zhou, Y., Nelson, J. S., & Lavernia, E. J. (2001). Theoretical and experimental analysis of droplet diameter, temperature, and

evaporation rate evolution in cryogenic sprays. *International Journal of Heat and Mass Transfer*, *44*(17), 3201-3211

[37] Lewis, S. R., Anumolu, L., & Trujillo, M. F. (2013). Numerical simulations of droplet train and free surface jet impingement. *International Journal of Heat and Fluid Flow*, *44*, 610-623

[38] Trujillo, M. F., Alvarado, J., Gehring, E., & Soriano, G. S. (2011). Numerical simulations and experimental characterization of heat transfer from a periodic impingement of droplets. *Journal of Heat Transfer*, *133*(12), 122201

[39] Soriano, G. E., Zhang, T., & Alvarado, J. L. (2014). Study of the effects of single and multiple periodic droplet impingements on liquid film heat transfer.*International Journal of Heat and Mass Transfer*, *77*, 449-463

[40] Fest-Santini, S., Guilizzoni, M., Santini, M., & COSSALI, G. (2012). Water drop impact into a deep pool: influence of the liquid pool temperature. In *DIPSI Workshop 2012. Droplet Impact Phenomena & Spray Investigations* (pp. 16-22). Dip. Ingegneria industriale. Università degli studi di Bergamo

[41] Anderson, R. P., & Ortega, A. (2009, January). Experiments and modeling of a liquid droplet transported by a gas stream impinging on a heated surface: single phase regime. In *ASME 2009 InterPACK Conference collocated with the ASME 2009 Summer Heat Transfer Conference and the ASME 2009 3rd International Conference on Energy Sustainability* (pp. 229-237). American Society of Mechanical Engineers

[42] Anderson, R. P., & Ortega, A. (2009, January). Experiments and Modeling of a Liquid Droplet Transported by a Gas Stream Impinging on a Heated Surface: Evaporative Regime. In *ASME 2009 International Mechanical Engineering Congress and Exposition* (pp. 1647-1654). American Society of Mechanical Engineers

[43] Rein, M. (1996). The transitional regime between coalescing and splashing drops. *Journal of Fluid Mechanics*, *306*, 145-165

[44] Thomson, J. J., & Newall, H. F. (1885). On the formation of vortex rings by drops falling into liquids, and some allied phenomena. *Proceedings of the royal society of London*, *39*(239-241), 417-436

[45] Watanabe, Y., Saruwatari, A., & Ingram, D. M. (2008). Free-surface flows under impacting droplets. *Journal of Computational Physics*, *227*(4), 2344-2365